Division of Engineering
BROWN UNIVERSITY
PROVIDENCE, R. I.

Summary of THEORETICAL AND EXPERIMENTAL INVESTIGATION OF GRATING TYPE, SILICON PHOTOVOLTAIC CELLS

Report Prepared by: L. Y. Chen

Work performed by: L. Y. Chen
J. J. Loferski

Sponsored by:

National Aeronautics and Space Administration
NASA Grant NGR-40-002-093

June 1975

Summary of

Theoretical and Experimental Investigation of Silicon Grating Type Photovoltaic Cells

Report prepared by: L. Y. Chen

Work performed by: J. J. Loferski
L. Y. Chen

Division of Engineering, Brown University, Providence, R. I.

June 1975

Technical Report NGR-40-002-093/2 to

the National Aeronautics and Space Administration

ABSTRACT

This report summarizes the work performed under NASA Grant NGR-40-002-093 on the theoretical and experimental aspects of single crystal, silicon photovoltaic devices made by forming a grating pattern of p/n junctions on the light receiving surface of the base crystal. Based on the general semi-conductor equations, a mathematical description is presented for the photovoltaic properties of such grating-like structures in a two-dimensional form. The resulting second order elliptical equation is solved by computer modeling to give solutions for various, reasonable, initial values of bulk resistivity, excess carrier concentration, and surface recombination velocity. The validity of the computer model is established by comparison with p/n devices produced by alloying an aluminum grating pattern into the surface of n-type silicon wafers. Current voltage characteristics and spectral response curves are presented for cells of this type constructed on wafers of different resistivities and orientations. Grating type cells are found to have increased spectral response to the high energy (blue) photo region of the solar spectrum, and short circuit currents equal to or greater than those of commercial cells. Cells produced to date have displayed open circuit voltages approximately 10 per cent less than those of commercial cells.

TABLE OF CONTENTS

FIGURE CAPTIONS

Fig. 1 One-dimensional model for a conventional P/N photovoltaic cell.

Fig. 2 Top view of a 50 x 50 mil^2 small area grating cell with $2a = 5.1\ \mu m$, $2b = 63.6\ \mu m$.

Fig. 3 Computational model of a diffused grating cell.

Fig. 4 Base collection efficiency as obtained from a numerical and the exact solutions of a one-dimensional cell.

Fig. 5 Excess minority charge carrier distribution in the base region per unit volume per incident photon of the one-dimensional cell as specified in Fig. 4.

Fig. 6 Skin collection efficiency as obtained from a numerical and the exact solutions of the one-dimensional cell as specified in Fig. 4.

Fig. 7 Calculated collection efficiency of a grating cell with two different surface recombination velocities of the base material.

Fig. 8 Calculated collection efficiency for grating cells with fixed $b/a = 5$ and $a = 2\ \mu m$, $10\ \mu m$ respectively.

Fig. 9 A qualitative description of the collection efficiency for grating cells with a fixed value of b/a and different values of a.

Fig. 10 A qualitative description of the collection efficiency for grating cells with a fixed value of a and different values of b.

Fig. 11 Number of photons available outside the earth's atmosphere as a function of photon energy.

Fig. 12 Number of photons available outside the earth's atmosphere as a function of photon wavelength.

Fig. 13 Collection efficiency of a grating cell and a corresponding conventional cell as a function of photon wavelength.

Fig. 14 Collection efficiency of a grating cell and a corresponding conventional cell as a function of the optical absorption constant.

Fig. 15 Absorption spectra of a single crystal silicon at 300°K.

Fig. 16 A qualitative description of the base collection efficiency of grating cells with opaque grating lines. b/a = constant.

Fig. 17 A qualitative description of the base collection efficiency of grating cells with opaque grating lines. a = constant.

Fig. 18 The aluminum - silicon system.

Fig. 19 Test sample configuration.

Fig. 20 Open circuit voltage versus alloying temperature.

Fig. 21 Configuration of cells produced on a single wafer.

Fig. 22 Normalized spectral responses for cells on wafer II and a commercial solar cell with AR coating removed.

Fig. 23 Relative spectral responses for cells on wafer I. 2a = 5.1 μm, $I_{sc}(max) = 9.46\ mA/cm^2$.

Fig. 24 Relative spectral responses for cells on wafer III. 2a = 5.1 μm, $I_{sc}(max) = 23.9\ mA/cm^2$.

Fig. 25 Relative spectral responses for cells on wafer V. 2a = 5.1 μm, $I_{sc}(max) = 28.8\ mA/cm^2$.

Fig. 26 Relative spectral responses for cells on wafer VI. b/a ≈ 3.

Fig. 27 A 1-cm^2 grating structure cell, 2a = 7.5 μm, 2b = 127.2 μm

Fig. 28 I-V characteristic of a 1-cm^2 grating cell under simulated AMO illumination.

Fig. 29 Normalized spectral response of a 1-cm^2 grating cell.

Fig. 30 Dark forward I-V characteristic and reciprocal slope m vs. V curve of a 1-cm^2 grating cell.

Fig. 31 Diagrams used to illustrate the origin of surface channel near a p-n junction.

Fig. 32 Five-point scheme of the finite difference method.

Fig. 33 Discretilization of the unit cell of a grating cell with a = 2 μm, b = 10 μm.

1. INTRODUCTION

Since the first publication by researchers at Bell Telephone Laboratories describing the invention of the modern silicon Solar Battery in 1954[1], the silicon solar cells have continued to dominate the field of photovoltaic energy conversion. During the past 20 years, two important developments in cell structure have led to today's high efficiency silicon solar cells.

The first important development is the shallow junction cell[2,3]. The concept that the collection efficiency is maximized if a very shallow junction is used, taking into account the surface recombination velocity, was first pointed out by Loferski in 1956[4]. Earlier in 1954, Cummerow[5,6] studied the dependence of collection efficiency on junction depth, minority carrier diffusion length, optical constant, under the assumption that both front and back surfaces have infinite surface recombination velocities. During the period 1960-1961, several experimental and theoretical studies on the variation of the spectral response of cells with junction depth were published[7,8,9]. These studies showed that moving the junction closer to the surface improved the spectral response of the cell in the blue region and hence gave higher efficiencies, particularly in AM0 (air mass zero) sunlight.

The second important development is the gridded cell. It was pointed out in an early report of Chapin, Fuller and Pearson[1] that series resistance was a major cause of power loss in the initial cells made at Bell Telephone Laboratories. In early 1959, it was recognized that the incorporation of contact grid lines could greatly reduce the series resistance caused by the thin diffused layer; Wolf described the benefits derived

from contact grids in a paper published in 1960[10]. Grid contacts were quickly incorporated into the design of commercial cells[11].

Coupled with improvement in the base material properties (e.g., long minority carrier life time, in the 8 to 10μs range), the combination of the grid contacts and shallow junction depth resulted in an increase of cell efficiency from about 6% to about 10% in the period 1959-1961[11].

There are two inherent disadvantages associated with the shallow junction cells that limit the cell performance.

a) High surface recombination velocity. (Or according to a different theory developed by Lindmayer and Allison[12], the recombination of excess charge carriers generated by the blue-violet light is not controlled by front surface recombination, but by the presence of a "dead layer" just beneath the front surface with an extremely short life time. For a n on p cell having junction depth of 4,000Å, the n^+ layer formed by diffusion of phosphorous into the silicon has a heavily damaged layer or "dead layer" of about 1,500Å.)

b) Short minority carrier diffusion length in the diffused skin region.

Because of the high temperature diffusion process (over 1,000°C) and high impurity concentration (varies from about 10^{20} cm^{-3} at the surface to a value of about 10^{15} cm^{-3} at the junction less than 0.5 μm below the surface) incorporated into the skin region, the diffused skin region is characterized by a high value of surface recombination velocity (or according to Lindmayer and Allison[12], by the presence of a dead layer of about 1,500Å), and short bulk diffusion length; over 10^5 cm/sec. and 1 μm, respectively, as compared to values in excess of 100μm for bulk diffusion length in the base material and attainable surface recombination velocities of less than

10^3cm/sec. for silicon[13,14] (the surface recombination velocity in a thermally oxidized silicon (4.5×10^{15} phosphorous atoms/cm^3) structure studied by Grove[15] was found to be of the order of 5 cm/sec.).

It was these problems of the standard diffused silicon cell that motivated this investigation of "grating" type cells (see section 2.3). Unlike a standard diffused cell which has its front surface covered completely by a thin diffused skin region, a grating type cell would have part of its front surface covered by a grating of finely spaced fine grid lines which form a potential barrier with the base substrate. The grating structure junction could be a diffused p-n junction, an alloyed p-n junction or a Schottky barrier jucntion. In such a cell, most of the surface exposed to the incident light would be the "virgin" silicon constituting the base material. It was anticipated that low surface recombination velocities would be attainable on this material in addition to the long diffusion length in this region (over 100μm as compared with about 1μm in the diffused skin region), and that the "blue response" of the cell would be increased. Its red response would be relatively unaffected provided that the spacing between grid lines were smaller than the diffusion length in the base material.

The development of the theory of grating cell, of a fabrication procedure and the subsequent measurement of the characteristics of the cells are the subjects of the work reported here.

2. THEORY

2.1 General Governing Equations

In a semiconductor, the behavior of charge carriers is governed by a) Poisson's Equation, b) Space Charge Equation, c) Drift-Diffusion Equation, and d) Continuity Equation.

a) Poissons' Equation,

$$\nabla \cdot \vec{E} = \frac{\rho}{\varepsilon}$$

where $\vec{E}$ is the electric field, ρ the charge density, and ε the dielectric constant.

b) Space Charge Equation

$$\rho(\vec{r}) = q(p(\vec{r}) - n(\vec{r}) + N_+(\vec{r}) - N_-(\vec{r}))$$

where $\vec{r}$ is the position vector, p hole density, n free electron density, $N_+(N_-)$ localized, immobile positive (negative) charge density.

c) Drift-Diffusion Equation,

$$\vec{J}_p = q\mu_p \vec{E}p - qD_p \vec{\nabla}p$$

$$\vec{J}_n = q\mu_n \vec{E}n + qD_n \vec{\nabla}n$$

where $\vec{J}_p(\vec{J}_n)$ is the hole (electron) current density, $\mu_p(\mu_n)$ the hole electron) mobility, $D_p(D_n)$ the hole (electron) diffusion constant.

d) Continuity Equation,

$$\frac{\partial p}{\partial t} = -\frac{1}{q} \nabla \cdot \vec{J}_p - R_p + G_p$$

$$\frac{\partial n}{\partial t} = \frac{1}{q} \nabla \cdot \vec{J}_n - R_n + G_n$$

where $R_p(R_n)$ is the net rate of recombination for holes (electrons), $G_p(G_n)$ is the rate of generation of holes (electrons) due to non-thermal source, such as light irradiation, high energy particle bombardment.

For the steady-state, field free case in nondegenerate extrinsic material and under the assumption of low-level injection (i.e., $n', p' \ll n_o$

in n-type material, and n', p' << p_o in p-type material, where p'(n') is the excess hole (electron) density, $p_o(n_o)$ is the thermal equilibrium hole (electron) density), $R_p(R_n)$ may be expressed as p'/τ_p (n'/τ_n)[16]. The Drift-Diffusion Equation and the Continuity Equation can be combined into one so-called semiconductor diffusion equation, which has the form

$$D_p \nabla^2 p' - \frac{p'}{\tau_p} + G_p = 0 \quad \text{in n-type material} \qquad (2.1a)$$

$$D_n \nabla^2 n' - \frac{n'}{\tau_n} + G_n = 0 \quad \text{in p-type material} \qquad (2.1b)$$

where $\tau_p(\tau_n)$ is the minority charge carrier life-time in a n-(p-) type material.

2.2 One-Dimensional (Conventional) p-n Junction Photovoltaic Cell

In the case of the standard photovoltaic cell, the spectral response can be obtained by solving the differential equations in a one-dimensional model as shown in Fig. 1. Assume there is no reflection of the incident light from the front surface, the absorption of the incident photons with energy larger than the energy gap of cell material is goverened by Labmert's Law (i.e., equal layer of equal thickness absorbs an equal fraction of the light which traverses it), and the quantum yield is unity. Then the number of electron-hole pairs generated by light with wavelength λ per unit volume $G_p(G_n)$ in Eq. 2.1 is $\alpha N_o(\lambda)e^{-\alpha x}$, where α is the optical absorption constant of the material and is a function of wavelength, $N_o(\lambda)$ is the incident light flux density with wavelength λ in photons/unit area-sec.).

The junction is at a distnace ℓ below the front surface. The thickness of the wafer is b, and usually $b >> \ell$.

The one-dimensional form of Eq. 2.1 is

$$D_p \frac{\partial^2 p'}{\partial x^2} - \frac{p'}{\tau_p} + \alpha N_o e^{-\alpha x} = 0 \qquad \text{on the n-side} \tag{2.2a}$$

$$D_n \frac{\partial^2 n'}{\partial x^2} - \frac{n'}{\tau_n} + \alpha N_o e^{-\alpha x} = 0 \qquad \text{on the p-side} \tag{2.2b}$$

Boundary conditions must be specified for the junction and the surfaces of the cell. The case of the short-circuited junction (i.e., when there is no potential difference appearing across the junction, and the current output is equal to the light generated current) is considered. For the p/n cell (p-type surface, n-type base) shown in Fig. 1, the boundary condition at the junction for a short circuit junction has the form,

$$n'(\ell) = p'(\ell) = 0 \tag{2.3}$$

because according to the assumption of quasi-equilibrium, $n'(\ell) = n_{po}(e^{qV/kT}-1)$, $p'(\ell) = p_{no}(e^{qV/kT}-1)$[17], and $V = 0$, where V is the potential difference appearing across the junction, p_{no} (n_{po}) is the thermal equilibrium minority carrier concentation in n-(p-) material; and at the surface,

$$J_n(0) = qS_o n'(0) = qD_n \frac{dn'}{dx}\Big|_{x=0} \tag{2.4a}$$

$$J_p(b) = qS_b p'(b) = -qD_p \frac{dp'}{dx}\Big|_{x=b} \tag{2.4b}$$

where S_o, S_b are surface recombination velocities on the front and back surfaces respectively.

Only the case of a thin space charge region is considered here, therefore, we can neglect recombination, generation or scattering of the carriers in the p-n transition region, in which case Shockley's diode theory of the p-n junction is valid[18]. The electron and hole contributions to the

total current across the junction are given by:

$$J_n = qD_n \left.\frac{dn'}{dx}\right|_{\ell} \tag{2.5a}$$

$$J_p = -qD_p \left.\frac{dp'}{dx}\right|_{\ell} . \tag{2.5b}$$

The ratio of the short-circuit current to the incident photon flux of wavelength λ neglecting reflection is referred to as the collection efficiency Q at wavelength λ,

$$Q = \frac{J_n + J_p}{qN_o} = \frac{J_n}{qN_o} + \frac{J_p}{qN_o} = Q_{skin} + Q_{base} . \tag{2.6}$$

Its value specifies the number of electrons flowing through the cell per incident photon.

Solution of the above equations with the appropriate boundary conditions yields expressions for the skin and base contributions to the collection efficiency[7]:

$$Q_{skin} = \frac{1}{\alpha(1-\nu_n^2/\alpha^2)} (\beta_n \nu_n e^{\nu_n \ell} - \gamma_n \nu_n e^{-\nu_n \ell} - \alpha e^{-\alpha \ell}) \tag{2.7}$$

where

$$\beta_n = (e^{-\nu_n \ell}(h + \alpha) - e^{-\alpha \ell}(h + \nu_n))/\Delta_n$$

$$\gamma_n = (e^{-\alpha \ell}(h - \nu_n) - e^{\nu_n \ell}(h + \alpha))/\Delta_n$$

$$\Delta_n = e^{\nu_n \ell}(h + \nu_n) - e^{-\nu_n \ell}(h - \nu_n)$$

$$h = S_o/D_n$$

$$\nu_n = (D_n \tau_n)^{-1/2} = L_n^{-1} ,$$

and

$$Q_{base} = \frac{e^{-b\alpha}}{\alpha(1-\nu_p^2/\alpha^2)} (-\beta_p \nu_p e^{\nu_p (b-\ell)} + \gamma_p \nu_p e^{-\nu_p (b-\ell)} + \alpha e^{\alpha(b-\ell)}) \tag{2.8}$$

where

$$\beta_p = (e^{-\nu_p(b-\ell)}(h-\alpha) - e^{\alpha(b-\ell)}(h+\nu_p))/\Delta_p$$

$$\gamma_p = (e^{\alpha(b-\ell)}(h-\nu_p) - e^{\nu_p(b-\ell)}(h-\alpha))/\Delta_p$$

$$\Delta_p = e^{\nu_p(b-\ell)}(h+\nu_p) - e^{-\nu_p(b-\ell)}(h-\nu_p)$$

$$h = S_b/D_p$$

$$\nu_p = (D_p\tau_p)^{-1/2} = L_p^{-1}.$$

To obtain the I_{sc} (short-circuit current) when a cell is illuminated by a broad band source, this calculation must be repeated to obtain a collection efficiency value for each wavelength used for the illumination (because of variations in optical obsorption constant with wavelength). An integration must then be performed to account for the dependence of illumination intensity on wavelength.

2.3 Two-Dimensional Grating-Type Diffused p-n Junction Photovoltaic Cell

The diffused grating type cells are cells whose light receiving surface is not covered completely by a diffused junction; the surface is partially covered by a diffused grating or grids of collecting junctions. The top view of a grating-type cell is shown in Fig. 2.

The diffused grating lines have a width "2a" and the spacing between the centers of these lines is "2b". Because of the periodicity of the grating structure, the collection efficiency of a grating cell can be obtained by solving the semiconductor diffusion equations in a unit of width "b" as shown in Fig. 3 and also because there is little variation along the

direction of grid lines a two-dimensional model is adopted. (Note that here we use n-type material as base, because n-type material is more suitable for making alloyed p-n junction and Schottky barrier cells). The governing equations and the conditions to be satisfied on the boundaries of the unit cell are shown in this figure. Because the neighboring cells are identical, due to symmetry requirement, we have to have $\partial n'/\partial y$, $\partial p'/\partial y$ equal to zero at the boundaries between neighboring unit cells.

The two-dimensional diffusion equation,

$$U_{xx} + U_{yy} - \frac{U}{L^2} + \frac{\alpha N_o}{D} e^{-\alpha x} = 0 \qquad (2.9)$$

where U can be either n' or p', does not have a closed form solution as in the one-dimensional case. It is a second order elliptical equation which can be solved approximately by finite-difference techniques[19,20] which replace the continuum by a discrete model, thus reducing the problem to a system of simultaneous linear difference equations.

The matrix of the resulting matrix equation is real, symmetric, with positive diagonal entries and non-positive off-diagonal entries, and is irreducibly diagonally dominant (the same thing is true for one-dimensional diffusion equation).[19] In addition to these properties, it is also a sparse matrix, i.e., a large percentage of the entries of this matrix are zero, therefore, the problem can be more appropriately solved by iterative methods. Of all the iterative schemes for solving linear systems, the successive over-relaxation method has been one of the most widely used. Its simplicity and firm mathematical basis together with numerical experience accumulated over the years make it a convenient, efficient, and reliable method.[19,20] Therefore, the successive over-relaxation iterative method was chosen for the computation. (See Appendix)

In order to test the effectiveness of the computational method (successive over-relaxation iterative method), the response for a cell completely covered by a diffused region (one-dimensional case) was computed and the results were compared with the closed form solution which exists for that case.

Figure 4 compares the base responses based on the exact solution and on a numerical approximate solution for the one-dimensional case. The case $S_2 = \infty$ corresponds to the case of a metal contact covering the whole back surface. The curves show that the numerical approximate solution is very good for α larger than $2 \times 10^3 cm^{-1}$, however, the numerical approximation underestmates the low α response. The profiles of the excess carriers concentration per incident photon with α as a parameter, in the base region from the exact solution are shown in Fig. 5.* We can see that as α keeps increasing, the slope at the two ends of the profile increases first and then decreases, but we used the same discretilization scheme for all α in the numerical computation, that means this approximation scheme is more accurate for α with smaller slopes, and indeed, Fig. 4 reflects this.

---

*

$$p'(x) = \frac{\alpha N_o e^{-\alpha \ell}}{D_p\left(\frac{1}{L_p^2} - \alpha^2\right)} \left\{ \frac{e^{-\alpha(b-\ell)} - e^{\frac{b-\ell}{L_p}}}{e^{\frac{b-\ell}{L_p}} - e^{-\frac{b-\ell}{L_p}}} e^{-\frac{x}{L_p}} + \frac{e^{-\frac{b-\ell}{L_p}} - e^{-\alpha(b-\ell)}}{e^{\frac{b-\ell}{L_p}} - e^{-\frac{b-\ell}{L_p}}} \cdot e^{\frac{x}{L_p}} + e^{-\alpha x} \right\} \quad \text{for } \ell \leq x \leq b$$

Figure 6 compares the skin responses based on the exact solution and on a numerical approximation for the one-dimensional case. In this case the numerical solution deviates from the exact solution in the high α region. The reason for this is simply that as α increases, the variations of the profile of excess carriers in the diffused skin region gets larger and with the same discretilization scheme, the approximation becomes less accurate. If we use finer mesh spacing, the deviation could be smaller. Note that, in a grating cell, the fraction of the cell area covered by the grating collectors is a/b; consequently, the contribution to the spectral response from the diffused skin region is about a/b times of that for one-dimensional case and the error in total response is accordingly reduced.

These comparisons of the exact and numerical solution for the one-dimensional case provided an estimate of the reliability of calculated spectral response curves of grating cells. In the computation for diffused grating cells, the sample thickness was set at 100μm; the junction depth was set at 1μm; the minority diffusion length in the base L_{Base} = 300μm, in the skin L_{skin} = 1μm; the diffusion constant in the base and in the skin $D_{base} = D_{skin} = 10\ cm^2/sec.$ (for a p/n n-type cell, this corresponds a doping density $10^{15}\ cm^{-3}$ in base material and $10^{18}\ cm^{-3}$ in skin material). The surface recombination velocity of the diffused region was assigned value $S_1 = 10^5$ cm/sec., the surface recombination velocity of the base region was assigned values $S_2 = 0$ and $S_2 = 10^3$ cm/sec. The number of points imposed for discretilization was limited by the cost of the numerical computation, but we believe the computation results have supplied us with the maximum information needed. The main purpose of the computation was to determine how the overall response of a grating cell changes when the a/b ratio changes and how the response compares to that of a conventional diffused solar cell.

Figure 7 shows the results of the computation for b/a ratio = 5, a = 2μm, and the indicated values of surface recombination velocity S_2. The figure shows base response, the diffused grating (skin) response, and total response. It is reasonable to expect that if the value of S_2 is between 0 and 10^3 cm/sec, the corresponding curves should also fall between the curves for S_2 = 0 and $S_2 = 10^3$ cm/sec.

Figure 8 shows the response curves for cases in which b/a is kept at 5, but "a" is assigned two different values, viz., a = 2 and 10μm. The diffused grating (skin) responses for the two cases are essentially the same. The base response for a = 10μm is overall lower than that for a = 2μm for all α.

Figure 9 shows the qualitative description of the response behavior for fixed b/a ratio and different values of a, when all other parameters which affect the response are held constant. It shows that as "a" increases, the skin response remains the same, but base response decreases monotonically, for all α. Note that in this figure, the curves labeled 1 and 2 are taken from Figure 8, curve 3 is extropolated to lie between these two computed curves. Since b/a is fixed, the ratio between the number of hole-electron pairs generated by photons of energy ε (corresponds to an optical absorption constant $\alpha(\varepsilon)$ of the material) in the base region and those in the diffused grating (skin) region is also kept constant. However, the average distance carriers travel to the junction is essentially the same for the light generated minority carriers in the skin region and increases for those in the base region. In other words, the probability of recombination before reaching the junction remains the same for light generated minority carriers in the diffused skin region and increases for those in the base region, as "a" increases. Therefore, the skin response should remain the same, but base response should decrease monotonically for all α as "a" increases.

Figure 10 shows the qualitative description of the response behavior for fixed "a" and different "b/a" ratios. The skin response is roughly reduced to a value of "a/b" times the response for the corresponding one-dimensional case (b=a), because the number of minority carriers generated in the diffused grating (skin) region per incident photon, per units area (total exposed area) is reduced to a/b of the one-dimensional case, and the average distance for these carriers to travel to the junction remains the same. In the base region, as "b" becomes larger, the average distance for minority carriers to travel to the junction (generated by monochromatic light) increases, and this is true for carriers generated by monochromatic light of all wavelength in the useful range. However, there are two cases to consider,

a) for high energy photons, those for which α is high in the material, the number of minority carriers generated per unit area (total exposed area) increases rapidly (because when b=a, almost all carriers generated are in the skin, very few in the base, and when b=2a, suddenly more than half of these carriers generated are in the base);

b) for low energy photons, those for which α is low in the material, the number of minority carriers generated per unit area remains the same (because even when b=a, almost all of these carriers generated are in the base region). Therefore, the base response increases for high energy photons and decreases for low energy photons as b/a begins to increase from unity. Eventually, however, as "b" continues to increase, the average number of minority carriers generated per unit area by high energy photons approaches a constant value, and no longer is enough to compensate for the effect (more recombinations) caused by the increase of the average distance minority carriers must travel to a collecting junction. Thereafter, the base response starts to drop for

all α, as indicated in Fig. 10 for the case b>>a.

Note that in Fig. 10, the curve with $b=b_2$ is reproduced from Fig. 7 for the case $S_2 = 0$, the curve with $b = b_o$ is the exact solution for the corresponding one-dimensional case. The other curves have been plotted qualitatively according to the reasoning above.

In order to compare the overall collection efficiency of a diffused grating and a corresponding one-dimensional cells under AMO illumination, the short circuit current for both cells are calculated from the integral:

$$I_{SC} = q \int_{1.12eV}^{\infty} \eta(\varepsilon) N_{\varepsilon}(\varepsilon) d\varepsilon \tag{2.10}$$

where 1.12eV is the energy gap of single crystal silicon at room temperature, $N_{\varepsilon}(\varepsilon)$ is the photon flux density in AMO spectrum ε is the photon energy, $\eta(\varepsilon)$ is the cell response to a photon of energy ε. $N_{\varepsilon}(\varepsilon)$ as shown in Fig. 11 was computed by Wysocki[21] from Johnson's data for the spectral irradiance at AMO.

For convenience in calculation, the Johnson curve of Fig. 11 was transformed into a curve of incident flux density as a function of wavelength λ, through the following relation:

$$N_{\lambda}(\lambda) d\lambda = -N_{\varepsilon}(\varepsilon) d\varepsilon \tag{2.11a}$$

$$N_{\lambda}(\lambda) = -N_{\varepsilon}(\varepsilon) \frac{d\varepsilon}{d\lambda} = -N_{\varepsilon}(\varepsilon) \left(-\frac{hc}{\lambda^2}\right) = N_{\varepsilon}(\varepsilon) \frac{\varepsilon}{\lambda} \tag{2.11b}$$

the resultant curve is shown in Fig. 12.

The response vs. photon wavelength for both the grating cell and the corresponding one-dimensional cell is shown in Fig. 13 which was transformed from Fig. 14 with the help of α vs. $h\nu$ curve (Fig. 15)[22,23]. Figure 14

shows the total response vs. α curves of the diffused grating cell whose response was calculated and displayed in Fig. 7 (the case b/a = 5, a = 2μm, $S_2 = 0$, S_2 is the surface recombination velocity of the "virgin" silicon between the grating lines, and a zero recombination velocity on the back surface), and the corresponding one-dimensional cell. By combining the information exhibited in Fig. 12 and Fig. 13, the short circuit current, from these two cells exposed to AMO sunlight can be computed by using the relation,

$$I_{SC} = q\int_0^{1.11\mu m} \eta(\lambda)N_\lambda(\lambda)\, d\lambda \quad . \tag{2.12}$$

The ratio of short circuits between the diffused grating cell and the corresponding one-dimensional cell is roughly 1.04. The response curve used for the diffused grating cell may seem to be a very favorable case, since in computing this curve, it is assumed that the surface recombination velocity $S_2 = 0$ for the "virgin" area, i.e., the area between grating lines. However, the grating structure used in the computation is not an optimized one and Fig. 7 shows that there is not much difference between curves with $S_2 = 10^3$ cm/sec. and $S_2 = 0$, and the value of S_2 attainable is expected to be much less than 10^3 cm/sec. (The surface recombination velocity in a thermally oxidized silicon structure studied by Grove[15] was found to be of the order of 5 cm/sec.).

The assumption that the back surfaces of these two cells have zero recombination velocity is for the simplication of computation, however, the order of magnitudes of these two short circuit currents is not expected to change if an infinite recombination velocity on back surfaces is used. Because for those carriers generated near the back-surface, they are dominated by the condition on the back surface, and as long as the optical absorption constant "α" does not change due to the incorporation of diffused grating

structure, the front structure of the cell would have little influence on those carriers generated near the back surface.

In summary, these calculations confirm that it is possible to design grating cells with higher short-circuit current circuit under AMO illumination, whose response at long wavelength is less than that of a corresponding conventional cell, but whose response at blue-ultraviolet region is larger. For a given conventional (one dimensional) cell, and a given minimum admissible value of "a", there are an infinite number of corresponding grating cells (in the sense that when "b" = "a", these grating cells become identical to the one-dimensional cell), a cell among all these cells with the highest I_{SC} under some certain illumination spectrum is called the optimized grating cell under that illumination. The optimized value of "b" would be strongly affected by the minority carrier diffusion length in the base region; for an exceedingly short base diffusion length, the optimized "b" may be even equal to "a".

2.4 Two-dimensional grating-type p-n junction photovoltaic cell with opaque grating lines

The structure of a grating type p-n junction photovoltaic cell with opaque grating lines is like that for a diffused grating type p-n junction cell, but with an opaque metal grating overlapping the grating structure p-n junction to form an ohmic contact; the junction can be either alloyed type or diffused type.

Assume that the metal grating is completely opaque, then the response comes only from the base region. For the case, "b"="a" (the cell is completely covered by the metal), the response vanishes. For the case "b">>"a" and "a"<<L_{base}, the grating intercepts only a small fraction of the light incident on the cell and the response is essentially the same as that of a diffused grating cell having the same grating structure. For intermediate values of

the b/a ratio and a << L_{Base}, the high α response of the base region is the same for the two cases, since for both cases it arises from absorption of photons in the near surface region of the base silicon between grating lines; the low α base response is approximately (b-a)/b times the diffused grating cell value, since it is assumed that the light incident normal to the surface continues to travel along this direction without deviation from its path, and the grating "shades" a/b of the exposed area. Because the light may not be normally incident and because of scattering the actual response of real opaque line grating cells for low α photons should lie between the dashed and the solid curves shown in Fig. 16 and Fig. 17.

Figure 16 is a qualitative description of the base spectral response behavior for opaque line grating cells with a fixed b/a ratio and different values of "a", which is obtained by modifying the base spectral responses of corresponding diffused p-n junction grating cells as shown in Fig. 9. Note that for low energy photons, the base response is approximately (b-a)/b of the value of that of a corresponding diffused p-n junction grating cell. In this figure, we have assumed b/a = 5.

Figure 17 is a qualitative description of the base spectral response behavior for opaque line grating cells with a fixed value of "a" and different values of b/a ratio, which is obtained by modifying the base spectral response of corresponding diffused p-n junction grating cells as shown in Fig. 10. Note that for low energy photons, the base response is approximately (b-a)/b of the value of that of a corresponding diffused p-n junction grating cell. In this figure, we have assumed $b_o = a$, $b_1 = 2a$, $b_2 = 5a$, $b_3 >> L_{Base}$.

From Figure 16, it is concluded that for a fixed "b/a" ratio, the response at all α decreases as "a" increases, and referring to Fig. 15

"absorption spectra of single crystal silicon at 300°K", it is equivalent to say that the response at all wavelength decreases as "a" increases. Therefore, under the illumination of some specific light source, if "b/a" ratio keeps constant, the short circuit current will decrease monotonically as "a" increases.

From Fig. 17, it is concluded that for fixed "a", the response at all α increases (referring to Fig. 15, it is equivalent to say that the response at all wavelength increases) as "b/a" begins to increase from unity, it will reach a maximum value at some certain value of "b", thereafter, the overall response will drop as "b" continues to increase, in contrast to the more complicated behavior for a diffused p-n junction grating cell as shown in the same figure. Therefore, for opaque line grating cells, if "a" is kept constant, the short circuit current will increase as "b/a" begins to increase from unity, it will reach a maximum value at some certain value of "b" (for a minimum admissible width of "a", this value of "b" depends on the minority carrier diffusion length, and on the surface recombination velocity of the base material), and will drop as "b" continues to increase.

2.5 Concerning possible methods for fabrication of grating type cells

A number of possible configurations of grating cells were considered. The diffused grating p-n junction cell can be made by using microelectronic techniques to define a diffused grating p-n junction pattern on a base wafer. The steps involved would be as follows. The surface of a n-(or p-) type Si single crystal wafer would be covered by a masking SiO_x layer. Photoresisting techniques would be used to define and etch the desired grating pattern into the oxide layer. The sample would be subjected to the standard diffusion process and a p-n junction grating pattern would be formed on the surface.

The wafer would again be covered by a masking SiO_x layer. Windows would be opened up in the SiO_x layer for deposition of ohmic constants to the diffused grating structure. These ohmic contacts could be fine metal lines, narrower than the diffused grating lines but forming a contact to every one of the diffused grating lines along its length. This method of fabrication of grating cells was attempted by others in our group[24]; we have concentrated on a simpler system, namely the alloyed-aluminum grating cell. The p-n junction grating pattern is formed not by diffusion, but rather by alloying Al into silicon. The aluminum network also constitutes the ohmic contact to the grating. Consequently the number of steps required to produce a grating cell is reduced. As we show below, it is even possible to omit the oxidation steps required to form a mask for the diffusion process. The aluminum alloying process requires heating the wafer up to the vicinity of 700°C for a few minutes; it would be preferable if this heating step could be eliminated or at least if the temperature were reduced. A Schottley barrier type grating cell would make this possible. The reverse saturation current I_o of a barrier type photovoltaic cell plays a very important role in setting the efficiency of a cell. It can be seen from a study of the simplified current-voltage characteristics of a barrier-type photovoltaic cell. The relationships between load current I and load voltage V has the form:

$$I = I_o \left(e^{qV/AkT} - 1\right) - I_{SC} \qquad (2.13)$$

where I_o is the reverse saturation current, I_{SC} is the light generated current; A is a constant whose value would be unity in a classical Schottley p-n junction but whose value in barriers formed on silicon lies between 1 and 2. In this expression the effects of internal series resistance R_S and

shunt resistance R_{sh} are neglected. From this equation, it follows that the open circuit voltage V_{oc} is given by

$$V_{oc} = \frac{AkT}{q} \ln\left(\frac{I_{sc}}{I_o} + 1\right) \tag{2.14}$$

The load voltage at the maximum power point V_{mp} is in turn given by

$$\left(1 + \frac{qV_{mp}}{AkT}\right) \exp\left(\frac{qV_{mp}}{AkT}\right) = \frac{I_{sc}}{I_o} + 1 \tag{2.15}$$

High efficiencies require high values of V_{mp} which in turn require low value of I_o. The value of I_{sc} should not depend on barrier height, provided that some sort of potential barrier is present. The value of I_o, however, is extremely sensitive to barrier height. In the case of the thermionic emission model[25] of a Schottky barrier junction

$$I_o \alpha \exp\left(-\frac{q\phi_\beta}{kT}\right) \tag{2.16}$$

Therefore, low values of I_o require high value of barrier height ϕ_β. The value of ϕ_β for gold on n-Si is about 0.8/eV[25], Au is a "lifetime killer" in Si, and therefore its employment in Si grating cells is undesirable in photovoltaic application. The value of ϕ_β for Al on n-Si is about 0.76 eV[26], however, a literature research showed that the reverse saturation current I_o for Au-n-Si Schottky barrier is significantly (several order) higher than that achieved in Si p-n junctions[27,28]. For Al-n-Si Schottky barrier junction, the I_o is even higher, it was for this reason that we chose to concentrate on alloyed aluminum p-n junction grating cells.

3. EXPERIMENT

3.1 Fabrication of aluminum-n-silicon alloy p-n junction cells

If an aluminum film is placed in contact with n-type silicon, and the resultant metal-semiconductor system is heated to its eutectic temperature (576°C) in a reducing atmosphere, there forms at the interface of the two materials a thin melt having the eutectic composition 11% silicon and 89% aluminum[29]. At this temperature, the molten region continues to enlarge, with the two components dissolved in the liquid phase at the eutectic composition, until the aluminum is exhausted. The aluminum is the limiting element because of the thinness of the aluminum film (less than 1μm) compared to the thickness of the silicon wafer (~250 μm), and the high percentage of aluminum in the eutectic composition.

As the aluminum-silicon system is heated above 576°C, the aluminum-silicon phase diagram (Fig. 18) shows that the percentage of silicon in the liquid phase increases. When the temperature of the system is lowered through the eutectic point, excess silicon in the liquid phase is rejected and a regrowth region forms at the liquid-silicon interface. The silicon base region acts as a seed for recrystallization of the rejected liquid silicon, and the regrown region is a single crystal with the same orientation as the undisturbed base region[30,31]. The phase diagram does not show it, but there is a small amount of aluminum which remains dissolved in silicon in the solid phase, approximately 7×10^{18} atoms/cm^3 [32]. Since the donor impurity concentrations in resistivities commonly used for solar cell manufacture, i.e., 100 ohm-cm to 0.01 ohm-cm, are in the range 10^{14} to 5×10^{18} atoms/cm^3, the regrowth region will be converted into p-type and an abrupt p-n junction will be formed at the regrowth region-base wafer interface.

The following steps have been followed in making Al-n-Si alloy p-n junction grating cells,

a) The prepolished n-silicon wafer having resistivity in the range 0.1 to 10 ohm-cm is cleaned in accordance with standard procedures commonly used for fabrication of microelectronic circuits (i) The wafer is cleaned ultrasonically in trichloroethylene for 30 sec., followed by cleaning in acetone for 30 sec. and in methanol for 30 sec. (ii) It is washed in a 1:1:5 solution of NH_4OH, H_2O_2 and deionized H_2O at 80°C for 15 min. (iii) It is washed in a 1:1:6 solution of HCL, H_2O_2 and deionized H_2O at 80°C for 15 min. (iv) It is rinsed in deionized H_2O. (v) It is dipped in buffered HF for 20 sec.).

b) A thin layer of aluminum (about 7,000Å) is deposited on the polished surface by vacuum evaporation at a pressure of about 5×10^{-6} torr.

c) Two thin layers, the first of titanium of a few hundred Å and the second of silver of about 1μm are deposited on the other side of the silicon wafer.

d) A layer of A-Z positive photoresist (AZ-111, Shipley Company, Inc., Newton, Mass.) is spread over the aluminum covered surface.

e) The photoresist is exposed through a mask which defines the grating pattern or patterns.

f) The photoresist is developed with A-Z developer. It is found that the developer is alkaline based which removes both the photoresist and the aluminum from the regions which are intended to be the open spaces between the lines in the grating pattern. This eliminates the metal etch step.

g) The remaining photoresist is removed by dissolving in acetone, thus leaving behind on the wafer an aluminum pattern of the desired form.

h) The wafer is heated in a reducing atmosphere at temperature in the vicinity of or above, the silicon-aluminum eutectic temperature (576°C).

During the heating process the aluminum alloys with the silicon forming p-n junctions and the Ti-Ag layer forms an ohmic contact to the base.

i) Leads are attached by bonding Cu wires with "silver print" paint to the Al on the light receiving surface of the cell.

In order to explore the relationship between open circuit voltage V_o and heating process, a group of samples having the configuration shown in Fig. 19 were prepared. Twenty-one samples were prepared from each silicon wafer having a resistivity of 2-3.5 ohm-cm and a (100) surface.

After the pattern had been defined (as described above), the samples were subjected to two kinds of alloying schedules. In one of these the samples were heated "slowly", in the other, "rapidly". In the "rapid" heating experiments, the controller of the furnace was set at the desired temperature and the furnace was turned on. It was found that with the combination of furnace and controller used, the interior of the furnace could reach a temperature in the vicinity of 700°C in about five minutes. In the "slow" heating experiments, the controller setting was gradually increased up to the desired temperature; about 15 minutes were consumed in attaining 700°C.

In both cases, the steps in the alloying procedure were as follows. The sample was placed inside a quartz tube which passed through a tubular furnace. The sample was positioned so that it would be in the middle of the tubular furnace. The tube was sealed and was purged with N_2 gas for 15 minutes followed by H_2 for 15 minutes before the furnace was turned on. The H_2 gas continued to flow through the tube during the heating cycle until the temperature in the furnace had returned to room temperature.

In both the rapid and slow heating cycles, the furnace was shut off as soon as the furnace had reached the desired processing temperature, i.e., the sample was kept at its maximum temperature for a few minutes only.

The open circuit voltage V_{oc} was measured by exposing the cells to light from a tungsten iodide source coupled with a water filter intended to reduce the infrared content of the incident light. The intensity was about 100 mW/cm^2, the samples were measured in succession at the same position. The measurement was performed quickly to minimize temperature increases. The aluminum covered "squares" of Fig. 19 are opaque, a photovoltage is generated because carriers produced around the periphery of the junction can be collected.

It was found that the values of V_{oc} measured on junctions produced by the "rapid" heating process were higher than the values measured on junctions produced by the "slow" heating process. Figure 20 shows the measured value of V_{oc} for junctions produced by the "rapid" heating process. The curve exhibits a broad maximum with V_{oc} values in the vicinity of 500 mV for alloying temperature between 650 and 750°C.

3.2 Optimization of grating geometry

a) Cell design parameters

The response of the grating type cells was discussed in the "theory" sections. The analysis given in section 2.4 predicts that, for an opaque line grating cell, when the line width "2a" is fixed, the short circuit current I_{sc} will increase as b/a begins to increase from unity, and will reach a maximum value for certain line width "2b" (this value of 2b should depend on the value of 2a, and on the diffusion length and surface recombination velocity of the base material). It also predicts that when b/a ratio is fixed, I_{sc} of the opaque line grating cell should decrease monotonically as "a" increases.

In order to verify these points, alloyed Al-n-Si grating cells of two different configurations were constructed, the dimension of the individual cells and their geometrical arrangement on the base wafer is shown in Fig. 21.

In configuration 1, cells with a fixed line width "2a" and varied spacings were fabricated. The line width was set at the minimum line width which can be generated at Brown's Microelectronic Lab (about 5μm) and the spacing was varied between 30 and 250 μm. The area covered by the grating pattern were 50x50 $mils^2$. Six groups of three cells each were made on five n-Si wafers having different resistivities and orientation, viz., 0.1 ~ 0.3 ohm-cm <111>, 2 ~ 3.5 ohm-cm <100>, 5 ohm-cm <111>, 10 ohm-cm <111> , and 8 ~ 12 ohm-cm <100>. These wafers are designated as wafer I, wafer II, wafer III, wafer IV and wafer V respectively. The actual values of "2a" and "2b" are given in Table 1. Figure 2 is a picture of the top view of group 2 cells.

In configuration 2, cells with a fixed line spacing to line width (b/a) ratio and six different line width "2a" were constructed. The b/a ratio chosen is 3, and the value of "2a" ranges from 10 to 80 μm. Six groups of three cells each and three groups of 2 cells each were made on a n-Si wafer with 1 ~ 2 ohm-cm resistivity and <100> orientation, and this wafer is designated as wafer VI. Group 9 consisted of a two 50x50 $mils^2$ "picture" frame", i.e., no grating pattern covered the surface; they were used to estimate the effect caused by the boundary of small area cell. Group 7 and Group 8 have the same grating structure as Group 2 and Group 4, respectively; however, the former also have four grating lines at right angle to the main grating pattern. The actual value of "2a" the line width and "2b" the line spacing of these groups are given in Table 2.

All these cells were fabricated according to the "rapid" heating cycle described before.

b) Measurement of I_{sc}

The short circuit current I_{sc} of these cells were measured for each of these cells exposed to a tungsten iodide lamp. The light intensity was set at a value which resulted in a short-circuit current density of 26.3mA/cm^2 from a 2-cm^2 commercial silicon solar cell without anti-reflection coating. This value was chosen because the same commerical cell generated a short-circuit current density of 26.3mA/cm^2 when it was exposed to an AMO solar similator. The highest values of short circuit current for each of these groups on wafer I through wafer VI are recorded in Table I and Table 2. In Table 1, it is observed that wafer V and wafer IV have almost equal I_{sc} for corresponding (same "a", same "b") grating cells, this implies that their minority carrier diffusion lengths are almost identical. The implication is drawn because of the following reasons:

i) all the wafers were subjected to the same fabrication process, thus they are supposed to have identical surface condition and therefore the surface recombination velocity of the base material,

ii) all the wafers have a thickness of 250 μm ± 50 μm, in this range the cell thickness have little effect on collection efficiency; therefore the only major factor left that would affect the collection efficiency and consequently the I_{sc} of an opaque line grating cell is the minority carrier diffusion length in the base material.

Hence, by comparing the I_{sc} for corresponding grating cells in these wafers, it appears that the values of the diffusion length in the base material would vary according to the following descending order: wafer V,

wafer IV, wafer II, wafer III and wafer I, since this is the descending order of magnitude for the I_{sc} of corresponding grating cells in these wafers.

From Table 1, it is found that for 2a≃ 5 μm, the optimum line spacing "2b" for wafer V and wafer IV is ≥ 250 μm, for wafer II, it is about 127 μm, for wafer III, it is about 64 μm, and for wafer I, ≤ 32 μm.

Table 2 lists the I_{sc}'s for cells fabricated on wafer VI, with a fixed b/a ration = 3. It is evident from this table that as "a" increases, I_{sc} decreases monotonically. The only exception to this monotonic decrease is group 3, we attribute this deviation from the pattern to unspecified imperfections in the cells of this group. We also expect that the rate of decrease of I_{sc} with increasing "a" would have been faster than what showed in Table 2. This might be caused by the interference of the side lines of these grating cells. The length of each of these four side lines and grating lines of these 50x50 $mils^2$ grating cells is only 1,270 μm, and the line spacings have lengths as long as 127 μm and 254 μm; therefore the strictly two dimensional model is somewhat violated for these large spacing grating cells.

c) Spectral response measurement

A Jarrel-Ash monochromater and tungsten-iodide source were used to make spectral response measurement for all cells on the six wafers over the range 4,000Å ~ 10,000Å. The output of each cell tested was measured as a function of the wavelength of incident radiation and relative to the output of a standard cell whose spectral response was measured at NASA Lewis Research Center*. The results were plotted as response per photon and were normalized

---

*The author wishes to thank Dr. Henry Brandhorst and Mr. Russell Hart of NASA Lewis Research Center for arrangement and assistance in using their facilities.

to unity at peak response for each individual cell. All these cells have a common feature, viz., they are blue shifted cells. Figure 22 shows a representative case. It shows a normalized spectral response curve for a commercial solar cell with its antireflection coating removed and the normalized spectral responses for these cells on wafer II. All these small cells normalized responses are confined within two small horizontal bars as shown in the figure. It is evident that these grating cells have higher blue response and lower red response than that of a commerical silicon solar cell.

Since the normalized spectral response curves for individual cells on each wafer in general have the same shape, the relative spectral responses for cells on each wafer can be plotted by using their normalized spectral response curves and their short circuit currents as listed in Table 1 and Table 2. Typical results are shown in Figs. 23, 24, 25, and 26. Figure 23 shows the case of wafer I. For cells on wafer I, the spectral response decreases monotonically with increasing "b" for $b \geq 32$ μm; this means the optimal value of "b" for wafer I is ≤ 32 μm. We expect that for $b \geq 191$ μm, the spectral response would have continued to decrease and not reaching some limiting value as shown in the figure. The reason is because of the very short diffusion length of this base wafer (see discussions of section 3.2b), only those carriers generated near grating lines are contributing to the response, therefore the contribution to the response by side lines is increasingly important for cells with large value of 'b" (for b = 254 μm, there are only 4 grating line collectors in a 50x50 $mils^2$ cell). Figure 24 shows the case of wafer III. For cells on wafer III, the overall response reaches a maximum when "b" is about 64 μm, and decreases monotonically

as "b" continues to increase. Figure 25 shows the case of wafer V. For cells on wafer V, the overall response keeps increasing as "b" increases from 32 μm, the optimal value of "b" for this wafer is ≥ 254 μm. Figure 26 shows the case of wafer VI, for which b/a is fixed at about 3. For cells on this wafer, the overall response decreases monotonically as "a" increases.

In summary, these results confirm the qualitatively description shown in Fig. 16 and Fig. 17 (via a relation between α and λ shown in Fig. 15), and the statements in section 2.4, viz., i) for fixed b/a ratio, the overall spectral response decreases as "a" increases, ii) for fixed "a", the overall response increases as b/a begins to increase from unity, it will reach a maximum value at certain value of "b" (for wafer 1, this b is ≤ 32 μm, for wafer III, this b is about 64 μm, for wafer V, this b is ≥ 254 μm), thereafter, the overall response will drop as "b" continues to increase.

3.3 Fabrication and measurement of 1-cm^2 grating cells

Four 1-cm^2 grating cells were fabricated on a 2 ~ 3.5 ohm-cm, (100) plane of a n-silicon wafer by using the "repid" heating cycle described above. The grating pattern consists of 7.5 μm grating lines spaced 127.2 μm apart. Its magnified picture is shown in Fig. 27.

The outputs of these cells were measured under a simulated AMO Sunlight at NASA Lewis Research Center. The intensity was set at 136 mW/cm^2 and the spectral distribution is a good approximation to the AMO spectra. The I-V curve of a 1-cm^2 grating cell is shown in Fig. 28, which also includes the I-V curve of a 2-cm^2 commerical Si cell whose antireflection coating has been removed. (The current reading for the 2-cm^2 cell has been adjusted to current / cm^2).

The following point can be made. The 1-cm^2 grating cell produced a short circuit current comparable to and indeed a little greater than that produced by the commercial cell, (with an antireflection coating, both cells should produce I_{sc} about 1.4 times the uncoated cell values). However, the open circuit voltage of the grating cell (0.47 V) is smaller than that generated by the diffused commercial cell (0.55V). The maximum power point for this 1-cm^2 grating cell occurs at 0.34 volts and 22.5 mA, this corresponds to a measured maximum efficiency of about 5.6%. The commercial cell of Fig. 28 has a measured maximum efficiency of about 8% with its AR (antireflection) coating removed, it occurs at 0.45 volts and 24 mA. The addition of an AR coating usually increases output by a factor of 1.4. Thus the commerical cell with AR coating would be expected to have an efficiency of about 11.2% and the 1-cm^2 grating cell with AR coating would be expected to have an AMO efficiency of about 7.9%. As we noted above, the short circuit currents of these two cells are comparable, if I_o of the grating cell could be reduced, and therefore V_{oc} increased, the efficiency of the grating cell would be higher. Table 1 shows that the maximum I_{sc} per unit area obtained from a grating cell in our study is 28.8 mA/cm^2 for illumination by a tungsten iodide source whose intensity was set to produce the same current in the same commercial Si cell as it generated when it was exposed to the AMO solar simulator at NASA Lewis Research Center. The tungsten iodide lamp is deficient in the blue region when compared with the AMO spectrum so that it is possible that I_{sc} could even be higher than 28.8mA/cm^2 in AMO sunlights. If this same value of I_{sc} (28.8mA/cm^2) had been obtained in the 1-cm^2 grating cell, its maximum power output could be increased by 1.1 times, and therefore efficiency would be about 8.8% with AR coating. This indicates that the 1-cm^2 grating cell whose characteristics have been measured and shown

in Fig. 28 and Fig. 29 is not optimized, higher efficiencies are potentially attainable in grating cells. Figure 29 compares the spectral response of the 1-cm^2 grating cell to that of the commercial silicon cell whose I-V curve is shown in Fig. 28. As expected the grating cell is a blue shifted cell relative to the commerical diffused junction solar cell.

3.4 Discussion about open circuit voltage

It is a common practice to represent the I-V characteristic of a solar cell under illumination as

$$I = \sum_{n=1}^{m} I_{on} (\exp(qV/A_n kT) - 1) - I_{sc} \qquad (3.1)$$

where I_{on} is a constant with the dimension of current, kT/q is the thermal voltage (0.026 volts at room temperature), the factor A_n is a dimensionless number having a value larger than 1, I_{sc} is the light generated current.

However, if the dark current flowing in the p-n junction of a silicon solar cell consists of two components, viz. 1) the bulk diffusion current, and 2) the bulk recombination-generation current in the transition region, then the I-V characteristic of such a cell under illumination can be represented approximately in the form

$$I = I_{DO}(\exp(qV/kT) - 1) + I_{TO}(\exp(qV/2kT) - 1) - I_{sc} \qquad (3.2)$$

where the first and second terms on the right hand side of this equation are bulk diffusion current and bulk transition region recombination current respectively, and I_{DO}, I_{TO} are constants with the dimensions of current. The open circuit voltage V_{oc} can be obtained by solving the equation:

$$I_{DO}(\exp(qV_{oc}/kT) - T) + I_{TO}(\exp(qV_{oc}/2kT) - 1) = I_{sc} \qquad (3.3)$$

for a conventional silicon solar cell $I_{TO} >> I_{DO}$.

If the p-n junctions of a grating type cell have the same characteristics as the p-n junction of a corresponding conventional solar cell, then, it is obvious, that the I_{TO} of the grating cell is approximately a/b of the I_{TO} of the corresponding conventional cell, and I_{DO} (conventional cell) > I_{DO} (grating cell) > a/b $\cdot I_{DO}$ (conventional cell). Therefore, when the I_{sc}'s of the grating type cell and the corresponding conventional cell have the same value, then from Eq. 3.3 and the previous argument, it is obvious that the V_{oc} of the grating cell is larger than the V_{oc} of the corresponding conventional cell.

Unfortunately, the experimental results showed otherwise. The V_{oc}'s of grating cells made by methods described in section 3.1 are less than 0.5 volts which is considerably lower than 0.6 volts for convention p/n cell and 0.55 volts for conventional n/p cell. Figure 30 shows the dark I-V forward characteristics of a 1-cm^2 grating type cell and a commerical Si cell with its AR coating removed. It is reasonable to say that the excessive large forward current of the grating type cell might be caused by some other current component rather than the bulk diffusion current and the bulk transition region recombination current.

According to Sah[33,34], the current flowing in a semiconductor junction may be divided into four components according to the location of the recombination and generation of electrons and holes. These are: 1) the bulk recombination-generation or the diffusion current, 2) the bulk recombination generation current in the transition region, 3) the surface recombination-generation current in the transition region, and 4) the surface channel current. The current voltage relationship for these four current components may be approximated by $I = I_s \exp(qV/mkT)$ if $V > 4kT/q$. Analysis shows that the reciprocal slope m for the current components 1) to 3) lies between

1 and 2, while for the surface channel current component 4) m is greater than 2 for silicon junctions and may be larger than 4 for larger channels. Figure 31.a is used by Sah to describe the generation recombination locations for these four current components. During his investigation, he used a field plate to induce a channel on the surface near a junction. A surface channel is defined as a region near a p-n junction into which either electrons or holes from the other side of the junction can flow without having to climb a potential barrier.

Also shown in Fig. 30, are the reciprocal slopes m for the 1-cm^2 grating cell and the commercial cell as a function of forward voltage. For high voltages, the large m is due to the series resistance, but around 0.2 volts, the m for the grating cell is 3.5, and by the interpretation of Sah, it means that in this voltage range, the current is dominated by the recombination generation current in the channel. Note that for the commercial cell with AR coating removed, the m also exceeds 2, this has also been observed by Shockley and others[35,36].

As to the origin of a surface channel in an alloyed p-n junction grating cell, it might be explained as follows. In figure 31.b and figure 31.c we sketch the cross-sectional views of a unit composed of a grating line and underlaid substrate before and after the alloying process. The nonuniform profile of the p-n junction formed underneath the grating line is a result of chemical etching undercut effect on the grating lines. During the alloying process, a certain amount of silicon underneath the Al grating lines would mix with Al (e.g., the eutectic composition of Si and Al is 11% of Si and 89% of Al by weight), and the quantity of Si participating in this process is proportional to the thickness of the overlaid Al film. The p-n junction would form at the interface between the molten region and the solid Si

substrate. As a result, a very thin layer of heavily doped p+ region (about 10 ~ 100Å, the same magnitude as the width of an inversion layer) is formed along the edges of the grating line, it is a hole channel. Holes from the neighboring bulk p+ region would flow into this channel, a voltage drop would develop along the path of current flow due to the high resistivity of the channel. Part of the hole current would be used to supply the recombination current in the surface channel transition region, and might be set equal to the change of the current flowing along the channel. The recombination current in the surface channel transition region is voltage dependent, and is proportional to Sinh v/2, where v is the voltage difference across the surface channel transition region. Then, according to the analysis by Sah[33], the channel current may be proportional to Sinh(qV/4kT), where V is the voltage difference between the bulk p+ region and the substrate.

Shunting paths also could be responsible for the excessive large current in a grating type cell. Stirn[38] investigated the shunting paths in conventional cells, and concluded that the shunting paths were localized in nature, the most likely cause of these shunting paths would be scratches penetrating through the junction region since in commerical solar cells, junction is only 0.3 to 0.5 microns from the surface. For alloyed grating type cells studied in this investigation, extremely shallow junctions would be formed along the edges of the grating lines for reasons described in last paragraph; therefore, shunting paths would be formed most likely along the edges of grating lines.

A possible remedy to eliminate the excessive large forward current in a grating type cell would be to use ion implantation technique to make such a cell. Al atoms could be ion implanted into a n-type Si substrate through

a suitable mask to define a grating structure p-n junction, and by decreasing the energy of the ion beam, an Al grating structure ohmic contact overlapping the p-n junction could be also imposed. In so doing, because there is no lateral spreading of the dopant, no surface channel on extremely shallow junction could be formed through metullurgical interaction.

4. CONCLUDING REMARKS

a) The design principles and the underlying theory for the grating-type photovoltaic cell have been established.

b) The grating-type Si photovoltaic cell can have a comparable or even greater short-circuit current, and, at least, in theory, a higher open-circuit voltage than the conventional Si photovoltaic cell, it is a potentially higher efficiency cell.

c) The grating type cell is a blue-shifted cell relative to the conventional cell, it has higher response to blue-ultraviolet light and lower response to red-infrared light.

d) The low open-circuit voltage of the alloyed Al-Si p-n junction grating type cells studied in this investigation might be due to the formation of extremely shallow junction along the edges of grating lines.

5. APPENDIX

By using the five point formula and the integration method[19] of the finite difference approximation technique, the second order, self-adjoint elliptical partial differential equation:

$$-(P(x,y)W_x)_x - (P(x,y)W_y)_y + \sigma(x,y)W(x,y) = f(x,y) \quad (5.1)$$

can be replaced by a discrete model. The approximate value of $W(x_i,y_j)$, viz., $\omega(x_i,y_j)$, can be represented in terms of $\omega(x_{i-1},y_j)$, $\omega(x_{i+1},y_j)$, $\omega(x_i,y_{j-1})$, $\omega(x_i,y_{j+1})$, $\sigma(x_i,y_j)$, $f(x_i,y_j)$, $P(x_i,y_{j+1/2})$, $P(x_i,y_{j-1/2})$, $P(x_{i+1/2},y_j)$ and $P(x_{i-1/2},y_j)$. The positions and some of the symbols are shown in Fig. 32. For simplicity, $\omega(x_i,y_j)$ is designated as $\omega_{i,j}$, so are the other symbols. We have

$$\omega_{i,j} = \frac{1}{D_{i,j}}(L_{i,j}\omega_{i-1,j} + R_{i,j}\omega_{i+1,j} + T_{i,j}\omega_{i,j+1} + B_{i,j}\omega_{i,j-1} + S_{i,j}) \quad (5.2)$$

where

$$L_{i,j} = P_{i-1/2,j}\ \frac{K_{j-1}+K_j}{2h_{i-1}}, \quad R_{i,j} = P_{i+1/2,j}\ \frac{K_{j-1}+K_j}{2h_i},$$

$$T_{i,j} = P_{i,j+1/2}\ \frac{h_{i-1}+h_i}{2K_j}, \quad B_{i,j} = P_{i,j-1/2}\ \frac{h_{i-1}+h_i}{2K_{j-1}},$$

$$D_{i,j} = L_{i,j} + R_{i,j} + T_{i,j} + B_{i,j} + \sigma_{i,j}\ \frac{h_{i-1}+h_i}{2} \cdot \frac{k_{j-1}+k_j}{2},$$

$$S_{i,j} = f_{i,j}\ \frac{h_{i-1}+h_i}{2} \cdot \frac{K_{j-1}+K_j}{2}.$$

For the successive over-relaxation iterative scheme,

$$\omega_{i,j}^{(m+1)} = (1-\Omega)\,\omega_{i,j}^{(m)} + \Omega(L_{i,j}\omega_{i-1,j}^{(m+1)} + R_{i,j}\omega_{i+1,j}^{(m)} + T_{i,j}\omega_{i,j}^{(m)+1} + B_{i,j}\omega_{i,j-1}^{(m+1)} + S_{i,j})/D_{i,j} \quad (5.3)$$

where $\omega_{i,j}^{(m+1)}$ represents the approximate value of $W_{i,j}$ after m+1 iterations, Ω is the over-relaxation factor, 1.9 was adopted as the value of Ω in the computation.

For the computational model as shown Fig. 3, $p(x,y) = 1$, $\sigma(x,y) = -1/L_n^2$ (or $-1/L_p^2$), $f(x,y) = N_o \alpha e^{-\alpha x}/D$.

A mesh is imposed upon the unit cell as shown in Fig. 33 (for the case $a = 2.\mu m$, $b = 10\ \mu m$). Note that the mesh spacings are finer near the junction and the front light receiving surface, because the variation of carriers concentration there is more rapid than in other areas.

The approximate value of the excess minority carriers at each mesh point in the skin region is assigned by $U_{i,j}$ (i from 1 to 11, j from 1 to 14); and these in the base region is assigned by $U_{i,j}$ (i from 11 to 17, j from 1 to 13; and for i from 1 to 17, j from 14 to 21) and $V_{i,j}$ (i from 2 to 41, j from 1 to 4 and for i from 1 to 41, j from 5 to 13).

Because of the boundary conditions on the junction (n'=p'=0) skin region and base region constitute two independent systems, therefore the problem can be solved separately.

The general computation scheme is like this; first, an initial value (arbitrary, but a good guess can prompt the convergent rate) is assigned to $U_{i,j}$ (and $V_{i,j}$), then the iterative procedure according to Eq. 5.3 is started. The iterative step is from left to right and from bottom to top.

After each complete iteration cycle, a test is performed, to see if the value $U_{i,j}^{(m+1)}$ (and $V_{i,j}^{(m+1)}$) meet the set criterion at each mesh point:

$$\left|\frac{U_{i,j}^{(m+1)} - U_{i,j}^{(m)}}{U_{i,j}^{(m+1)}}\right| \left(\text{and } \left|\frac{V_{i,j}^{(m+1)} - V_{i,j}^{(m)}}{V_{i,j}^{(m+1)}}\right|\right) < \varepsilon \qquad (5.4)$$

If the answer is no, then the iteration process is continued, if the answer is yes, then it is proceeded to calculate the collection efficiency.

The calculation is done according to the following scheme:

$$Q_{skin} = \frac{I_{scs}}{qNo\ b} \quad , \quad Q_{base} = \frac{I_{scb}}{qNo\ b} \tag{5.5}$$

where I_{scs} is the short circuit current contributed by the skin region, I_{scb} is that contributed by the base region. No is the number of photons incident onto the cell, b is the half line spacing described in section 2.3. And:

$$I_{scs} = -qD_n \int_{junction} \vec{\nabla} n' \cdot d\vec{n}$$

$$\approx qD_n \left(\frac{1}{K_{13}} \sum_{i=1}^{10} h_i \frac{U_{i,13}+U_{i+1,13}}{2} + \frac{1}{h_{10}} \sum_{j=1}^{13} k_j \frac{U_{10,j}+U_{10,j+1}}{2} \right. \tag{5.6a}$$

$$I_{scb} = q\ D_p \int_{junction} \vec{\nabla} p' \cdot d\vec{n}$$

$$\approx qDp \left(\frac{1}{k_{14}} \sum_{i=1}^{10} h_i \frac{U_{i,15}+U_{i+1,15}}{2} + \frac{1}{h_{11}} \sum_{j=1}^{13} k_j \frac{U_{12,j}+U_{12,j+1}}{2} \right. \tag{5.6b}$$

where $\vec{n}$ is a unit vector normal to the surface of the region considered.

After the collection efficiency and the new values of $U_{i,j}$ (and $V_{i,j}$) are recorded, the whole process is repeated for several times with smaller ε's, until is is assured that the final result is a reasonably satisfactory one.

For example, for $\alpha = 2\text{x}10^3\ cm^{-1}$, the ε was set at $3\text{x}10^{-3}$, $1\text{x}10^{-3}$, $5\text{x}10^{-4}$, and $3\text{x}10^{-4}$ in this order and Q_{base} = 1.016 (after 72 iterations), 0.9521 (after 64 iterations), 0.9165 (after 137 iterations), and 0.9006 (after 196 iterations) correspondingly, it was deemed satisfactory, and the value 0.90 was taken as the approximated value of Q_{base}.

The following is a complete computer program used in the computation described above.

```
      DIMENSION U(17,33),HU(17,33),H(17),HK(33),
     1HL(17,33),R(17,33),T(17,33),D(17,33),S(17,33),
     1B(17,33),HL1(41,13),R1(41,13),T1(41,13),D1(41,13),S1(41,13),
     1B1(41,13),V(41,13),HV(41,13),G(41),GK(13),F(41),F1(41),
     1A1(3),A2(3),APHA(3),N(3)
      READ (5,100) KMAX,ERMAX
      READ (5,600) (A1(L),L=1,3),(A2(L),L=1,3),
     1(APHA(L),L=1,3),(N(L),L=1,3)
      READ (4) ((U(I,J),I=1,17),J=1,33),((V(I,J),I=1,41),J=1,13)
      L=3
      DO 19 I=1,12
   19 H(I)=0.1
      H(13)=0.2
      H(14)=0.2
      H(15)=0.4
      H(16)=0.5
      DO 20 J=1,7
   20 HK(J)=0.2
      DO 21 J=8,15
   21 HK(J)=0.1
      HK(16)=0.2
      HK(17)=0.2
      HK(18)=0.4
      DO 55 J=19,32
   55 HK(J)=0.5
      DO 22 I=1,10
   22 G(I)=1.
      DO 23 I=11,20
   23 G(I)=2.
      DO 24 I=21,36
   24 G(I)=4.
      G(37)=2.
      G(38)=2.
      G(39)=1.
      G(40)=1.
      GK(1)=0.4
      GK(2)=0.6
      GK(3)=0.5
      GK(4)=0.5
      DO 25 J=5,12
   25 GK(J)=1.
      F(1)=APHA(L)*10.**41
      DO 31 I=1,15
   31 F(I+1)=F(I)*EXP(-APHA(L)*H(I))
      DO 41 J=2,13
      DO 41 I=2,10
      HL(I,J)=(HK(J-1)+HK(J))/(2.*H(I-1))
      R(I,J)=(HK(J-1)+HK(J))/(2.*H(I))
      T(I,J)=(H(I-1)+H(I))/(2.*HK(J))
      B(I,J)=(H(I-1)+H(I))/(2.*HK(J-1))
      D(I,J)=HL(I,J)+R(I,J)+T(I,J)+B(I,J)
     1+(H(I-1)+H(I))*(HK(J-1)+HK(J))/(4.*1.*1.)
   41 S(I,J)=(H(I-1)+H(I))*(HK(J-1)+HK(J))*F(I)/4.
```

```
      K=0
   30 K=K+1
      DO 32 J=1,13
   32 U(1,J)=10.*U(2,J)/11.
      DO 33 I=1,10
   33 U(I,1)=U(I,2)
      DO 34 J=2,13
      DO 34 I=2,10
      HU(I,J)=U(I,J)
   34 U(I,J)=1.9*(S(I,J)+HL(I,J)*U(I-1,J)+R(I,J)*U(I+1,J)
     1+T(I,J)*U(I,J+1)+B(I,J)*U(I,J-1))/D(I,J)+(1.-1.9)*U(I,J)
      DO 35 J=2,13
      DO 35 I=2,10
      ER=ABS(U(I,J)-HU(I,J))/U(I,J)
      IF (ER-ERMAX) 35,39,39
   35 CONTINUE
      WRITE (6,200) K,(U(I,13),I=1,10)
      WRITE (6,200) K,(U(10,J),J=1,13)
      TU=0.
      DO 37 I=1,10
   37 TU=TU+(U(I,13)+U(I+1,13))*H(I)/2.
      DO 38 J=1,13
   38 TU=TU+(U(10,J)+U(10,J+1))*HK(J)/2.
      TUP=TU*10./(10.*10.**41)
      WRITE (6,300) K,TUP
      GO TO 50
   39 IF (K .LE. KMAX) GO TO 30
      WRITE (6,200) KMAX
   50 F(1)=APHA(L)*10.**41
      DO 67 I=1,15
   67 F(I+1)=F(I)*EXP(-APHA(L)*H(I))
      DO 42 J=2,14
      DO 42 I=12,16
      HL(I,J)=(HK(J-1)+HK(J))/(2.*H(I-1))
      R(I,J)=(HK(J-1)+HK(J))/(2.*H(I))
      T(I,J)=(H(I-1)+H(I))/(2.*HK(J))
      B(I,J)=(H(I-1)+H(I))/(2.*HK(J-1))
      D(I,J)=HL(I,J)+R(I,J)+T(I,J)+B(I,J)
     1+(H(I-1)+H(I))*(HK(J-1)+HK(J))/(4.*300.*300.)
   42 S(I,J)=(H(I-1)+H(I))*(HK(J-1)+HK(J))*F(I)/4.
      DO 43 J=15,32
      DO 43 I=2,16
      HL(I,J)=(HK(J-1)+HK(J))/(2.*H(I-1))
      R(I,J)=(HK(J-1)+HK(J))/(2.*H(I))
      T(I,J)=(H(I-1)+H(I))/(2.*HK(J))
      B(I,J)=(H(I-1)+H(I))/(2.*HK(J-1))
      D(I,J)=HL(I,J)+R(I,J)+T(I,J)+B(I,J)
     1+(H(I-1)+H(I))*(HK(J-1)+HK(J))/(4.*300.*300.)
   43 S(I,J)=(H(I-1)+H(I))*(HK(J-1)+HK(J))*F(I)/4.
      F1(1)=APHA(L)*10.**41
      M=N(L)
      DO 71 I=1,M
   71 F1(I+1)=F1(I)*EXP(-APHA(L)*G(I))
      DO 72 I=M,39
   72 F1(I+2)=0.
```

```
      DO 44 J=2,12
      DO 44 I=4,40
      HL1(I,J)=(GK(J-1)+GK(J))/(2.*G(I-1))
      R1(I,J)=(GK(J-1)+GK(J))/(2.*G(I))
      T1(I,J)=(G(I-1)+G(I))/(2.*GK(J))
      B1(I,J)=(G(I-1)+G(I))/(2.*GK(J-1))
      D1(I,J)=HL1(I,J)+R1(I,J)+T1(I,J)+B1(I,J)
     1+(G(I-1)+G(I))*(GK(J-1)+GK(J))/(4.*300.*300.)
   44 S1(I,J)=(G(I-1)+G(I))*(GK(J-1)+GK(J))*F1(I)/4.
      K=0
   60 K=K+1
      DO 61 I=12,16
   61 U(I,1)=U(I,2)
      DO 62 J=15,33
   62 U(1,J)=10.*U(2,J)/10.01
      DO 63 I=4,40
   63 V(I,1)=V(I,2)
      DO 64 I=4,40
   64 V(I,13)=V(I,12)
      DO 65 I=1,16
   65 U(I,33)=U(I,32)
      U(17,1)=(V(4,1)+U(16,1))/2.
      U(17,3)=(V(4,2)+U(16,3))/2.
      U(17,2)=(U(17,3)+U(17,1))/2.
      U(17,6)=(V(4,3)+U(16,6))/2.
      E=U(17,6)-U(17,3)
      U(17,4)=U(17,3)+0.333*E
      U(17,5)=U(17,3)+0.666*E
      U(17,9)=(V(4,4)+U(16,9))/2.
      E=U(17,9)-U(17,6)
      U(17,7)=U(17,6)+0.4*E
      U(17,8)=U(17,6)+0.8*E
      U(17,14)=(V(4,5)+U(16,14))/2.
      E=U(17,14)-U(17,9)
      U(17,10)=U(17,9)+0.2*E
      U(17,11)=U(17,9)+0.4*E
      U(17,12)=U(17,9)+0.6*E
      U(17,13)=U(17,9)+0.8*E
      U(17,19)=(V(4,6)+U(16,19))/2.
      E=U(17,19)-U(17,14)
      U(17,15)=U(17,14)+0.1*E
      U(17,16)=U(17,14)+0.2*E
      U(17,17)=U(17,14)+0.4*E
      U(17,18)=U(17,14)+0.6*E
      DO 66 J=1,7
      U(17,19+2*J)=(V(4,6+J)+U(16,19+2*J))/2.
   66 U(17,19+2*J-1)=(U(17,19+2*J)+U(17,19+2*J-2))/2.
      DO 68 J=2,14
      DO 68 I=12,16
      HU(I,J)=U(I,J)
   68 U(I,J)=1.9*(S(I,J)+HL(I,J)*U(I-1,J)+R(I,J)*U(I+1,J)
     1+T(I,J)*U(I,J+1)+B(I,J)*U(I,J-1))/D(I,J)+(1.-1.9)*U(I,J)
      DO 69 J=15,32
      DO 69 I=2,16
      HU(I,J)=U(I,J)
```

```
 69 U(I,J)=1.9*(S(I,J)+HL(I,J)*U(I-1,J)+R(I,J)*U(I+1,J)
   1+T(I,J)*U(I,J+1)+B(I,J)*U(I,J-1))/D(I,J)+(1.-1.9)*U(I,J)
    DO 13 J=1,13
 13 V(41,J)=V(40,J)
    V(3,1)=U(16,1)
    V(3,2)=U(16,3)
    V(3,3)=U(16,6)
    V(3,4)=U(16,9)
    V(3,5)=U(16,14)
    V(3,6)=U(16,19)
    DO 70 J=1,7
 70 V(3,6+J)=U(16,19+2*J)
    DO 73 J=2,12
    DO 73 I=4,40
    HV(I,J)=V(I,J)
 73 V(I,J)=1.9*(S1(I,J)+HL1(I,J)*V(I-1,J)+R1(I,J)*V(I+1,J)
   1+T1(I,J)*V(I,J+1)+B1(I,J)*V(I,J-1))/D1(I,J)+(1.-1.9)*V(I,J)
    DO 74 J=2,14
    DO 74 I=12,16
    ER=ABS(U(I,J)-HU(I,J))/U(I,J)
    IF (ER-ERMAX) 74,80,80
 74 CONTINUE
    DO 75 J=15,32
    DO 75 I=2,16
    ER=ABS(U(I,J)-HU(I,J))/U(I,J)
    IF (ER-ERMAX) 75,80,80
 75 CONTINUE
    DO 76 J=2,12
    DO 76 I=4,40
    ER=ABS(V(I,J)-HV(I,J))/V(I,J)
    IF (ER-ERMAX) 76,80,80
 76 CONTINUE
 81 TU=0.
    DO 77 I=2,11
 77 TU=TU+(U(I,15)+U(I-1,15))*H(I-1)/2.
    DO 78 J=2,14
 78 TU=TU+(U(12,J)+U(12,J-1))*HK(J-1)/2.
    TUN=TU*10./(10.*10.**41)
    WRITE (6,400) K,TUN
    WRITE (6,200) K,(U(12,J),J=1,33,2)
    WRITE (6,200) K,(U(I,15),I=1,17)
    WRITE (6,200) K,(U(I,25),I=1,17,2),(V(I,9),I=4,40,2)
    WRITE (6,200) K,(U(I,19),I=1,17,2),(V(I,6),I=4,40,2)
    WRITE (6,200) K,(U(I,14),I=12,17),(V(I,5),I=4,40,2)
    WRITE (6,200) K,(U(I,6),I=12,17),(V(I,3),I=4,40,2)
    WRITE (6,200) K,(V(11,J),J=1,13)
    WRITE (4) ((U(I,J),I=1,17),J=1,33),((V(I,J),I=1,41),J=1,13)
    GO TO 90
 80 IF (K .LE. KMAX) GO TO 60
    GO TO 81
 90 CONTINUE
    STOP
100 FORMAT (I10,F10.4)
200 FORMAT (I10/7E12.4/7E12.4/7E12.4/7E12.4/7E12.4)
300 FORMAT (I10/5H TUP=,E12.4)
```

```
400 FORMAT (I10/5H TUN=,E12.4)
600 FORMAT (3E10.2/3E10.2/3E10.2/3I10)
    END
```

6. REFERENCES

1. Chapin, D. M., Fuller, C. S., Pearson, G. L., J. Appl. Phys. 25, 676 (1954).
2. Prince, M., J. Appl. Phys. 26, 534 (1955).
3. Wolf, M., IEEE, the 8th Photovoltaic Specialists Conference Record, 361 (1970).
4. Loferski, J. J., J. Appl. Phys. 27, 777 (1956).
5. Cummerow, R., Phys. Rev., 95, 16 (1954).
6. Cummerow, R., Phys. Rev., 95, 561 (1954).
7. Loferski, J. J., Wysocki, J. J., RCA Review, 22, 38 (1961).
8. Terman, L. M., Solid State Electronics 2, 1 (1961).
9. Wolf, M., Solar Energy 5, 83 (1961).
10. Wolf, M., Proc. IRE, 48, 1246 (1960).
11. Matlaw, S. L., Ralph, E. L., J. Appl. Phys., 30, 541 (1959).
12. Lindmayer, J., Allison, J., COMSAT Tech. Rev., 3, 1 (1973).
13. Loferski, J. J., Ranganathan, N., Crisman, E. E., Second Semiannual Report on NASA Grant 40-002-093, Division of Engineering, Brown University.
14. Loferski, J. J., Ranganathan, N., Crisman, E. E., Third Semiannual Report on NSAS Grant NGR 40-002-093, Division of Engineering, Brown University.
15. Grove, A. S., Fitzgerald, D. J., Solid State Electron 9, 783 (1966).
16. Shockley, W., Read, W. T. Jr., Phys. Rev. 87, 835 (1952).
17. Grove, A. S., Physics and Technology of Semiconductor Devices, (John Wiley & Sons, Inc., 1967).
18. Shockley, W., Bell Syst. Tech. J., 28, 435 (1949).
19. Varga, R. S. , Marrix Iterative Analysis, (Prentice-Hall, Inc., 1962).
20. Wackspress, E. L., Iterative Solution of Elliptic Systems, (Prentice-Hall Inc., 1966).

21. Wysocki, J. J., Solar Energy 6, 104 (1962).

22. Dash, W. C., Newman, R., Phys. Rev. 99, 1151 (1955).

23. Philipp, H. R., Taft, E. A., Phys. Rev. Letters 8, 13 (1962).

24. Loferski, J. J., Roessler, B., Crisman, E. E., Chen, L. Y., Kaul, R., Walker, J., Ninth Semiannual Report on NSAS Grant NGR 40-002-093, Division of Engineering, Brown University.

25. Van Der Ziel, A., Solid State Physical Electronics, (Prentice Hall, Ind., 1968).

26. Turner, M. J., Rhoderick, E. H., Solid State Electron 11, 291 (1968).

27. Lepselter, M. P., Sze, S. M., Bell Syst. Tech. J. 47, 195 (1968).

28. Polgar, P., Mouyard, A., Shiner, B., IEEE Trans. Elect. Dev. ED-17, 725 (1970).

29. Hansen, M., Anderko, A., Constitution of Binary Alloys, (McGraw-Hill, 1958).

30. Saby, J. S., Dunlop, W. C., Jr., Phys. Rev. 90, 630 (1953).

31. Biondi, F. J., Editor, Transistor Technology, Vol. III, Chapt. 7, (D. Van Nostrand Company, Inc., 1958).

32. Trumbore, F. A., Bell Syst. Tech. J. 39, 205 (1960).

33. Wolf, M., Ralph, E. L., IEEE Trans. Elect. Dev. ED-12, 470 (1965).

34. Sah, C. T., Proc. IRE, 49, 1623 (1961).

35. Sah, C. T., IRE Trans. Elect. Dev. ED-9, 94 (1962).

36. Shockley, W., Queisser, H. J., J. Appl. Phys. 32, 510 (1961).

37. Wolf, M., IEEE Eighth Photovoltaic Specialists Conference, August, 1970, Conference Record, pp. 360-371.

38. Stirn, R. I., IEEE Ninth Photovoltaic Specialists Conference, May, 1972, Conference Record, pp. 72-82.

TABLE I

GROUP NUMBER	CELL NUMBERS	2a (μm)	2b (μm)	I_{sc} (mA/cm^2)				
				WAFER I 0.1-0.3Ω-cm <111>	WAFER II 2-3.5Ω-cm <100>	WAFER III 5Ω-cm <111>	WAFER IV 10Ω-cm <111>	WAFER V 8-12Ω-cm <100>
1	1, 7, 13	5.1	31.8	9.46	24.7	23.3	25.2	25.2
2	2, 8, 14	5.1	63.5	8.40	25.8	23.9	27.0	27.2
3	3, 9, 15	5.1	95.3	5.45	25.6	20.5	26.9	26.1
4	4, 10, 16	5.1	127.6	3.97	27.9	16.7	27.2	28.6
5	5, 11, 17	5.1	190.8	3.01	26.8	11.8	27.1	27.5
6	6, 12, 18	5.1	254.4	3.07	26.7	6.98	28.6	28.8

TABLE 2

GROUP NUMBER	CELL NUMBERS	2a (μm)	2b (μm)	I_{sc} (mA/cm^2) WAFER 1~2 Ω-cm <100>
1	1,7,13	10.2	31.8	24.2
2	2,8,14	20.4	63.6	22.7
3	3,9,15	30.6	95.4	21.2
4	4,10,16	40.8	127.2	21.9
5	5,11,17	61.2	190.8	19.6
6	6,12,18	81.6	254.4	19.3
7*	19,22	20.4	63.6	19.7
8*	20,23	40.8	127.2	16.6
9	21,24			8.4

* WITH FOUR HORIZONTAL BARS ACROSS THE GRATING LINES

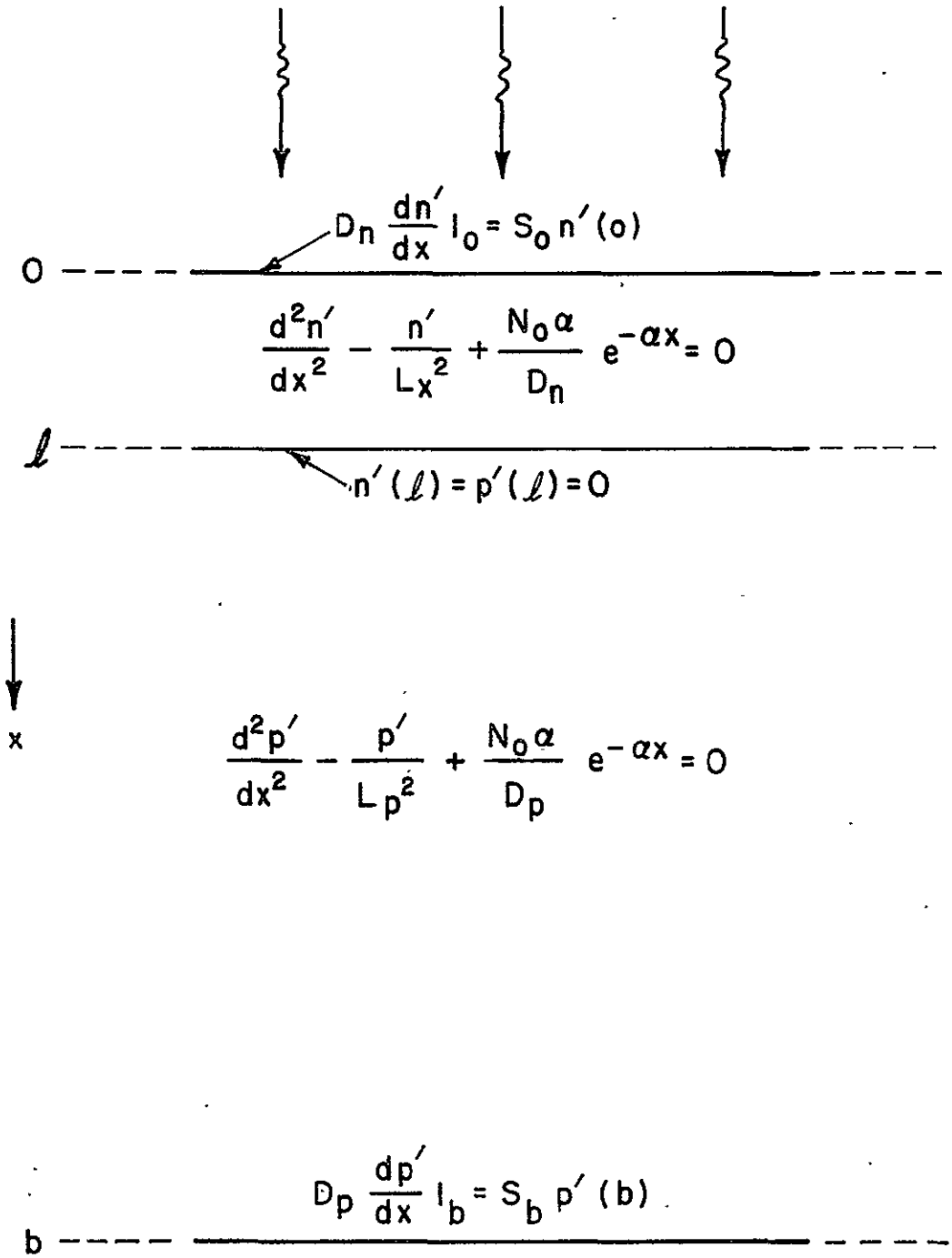

FIG. 1 ONE DIMENSIONAL MODEL FOR A CONVENTIONAL P/N PHOTOVOLTAIC CELL.

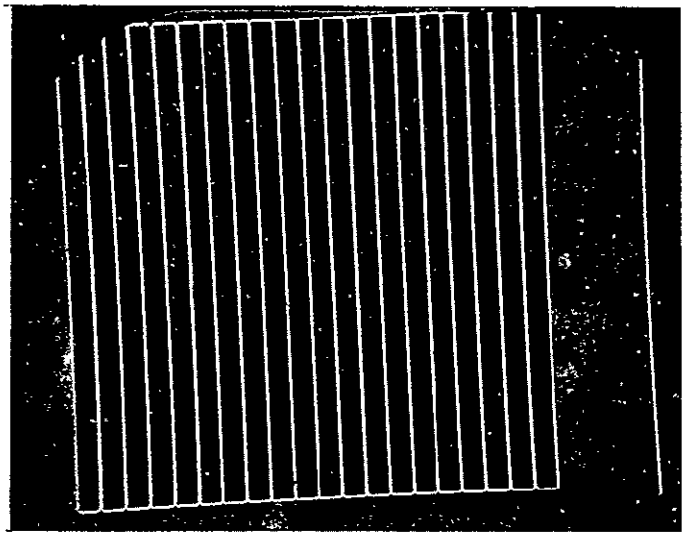

FIG. 2 TOP VIEW OF A 50 × 50 MIL^2 SMALL AREA GRATING CELL WITH $2a = 5.1\mu m$, $2b = 63.6\mu m$.

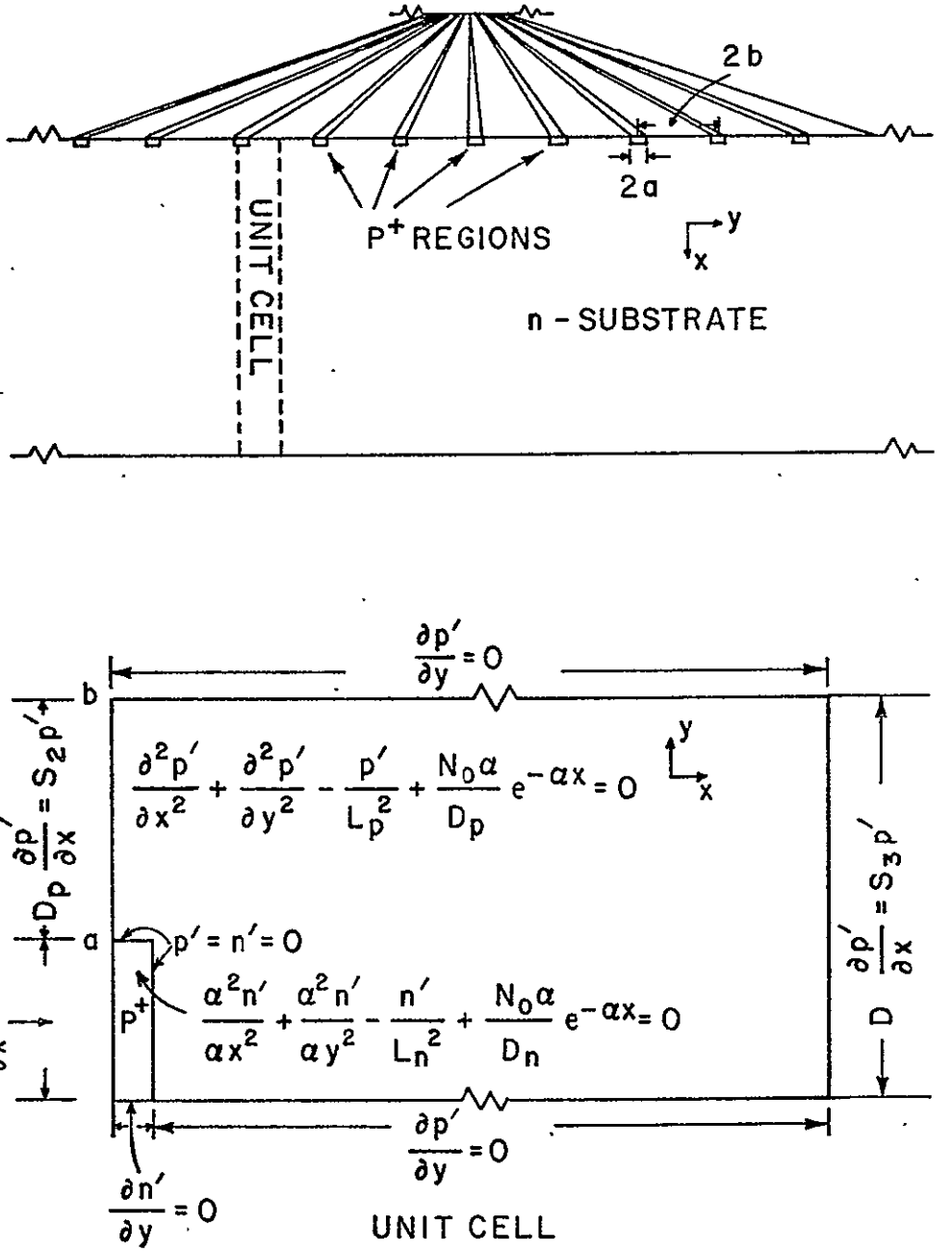

FIG. 3 COMPUTATIONAL MODEL OF A DIFFUSED GRATING CELL.

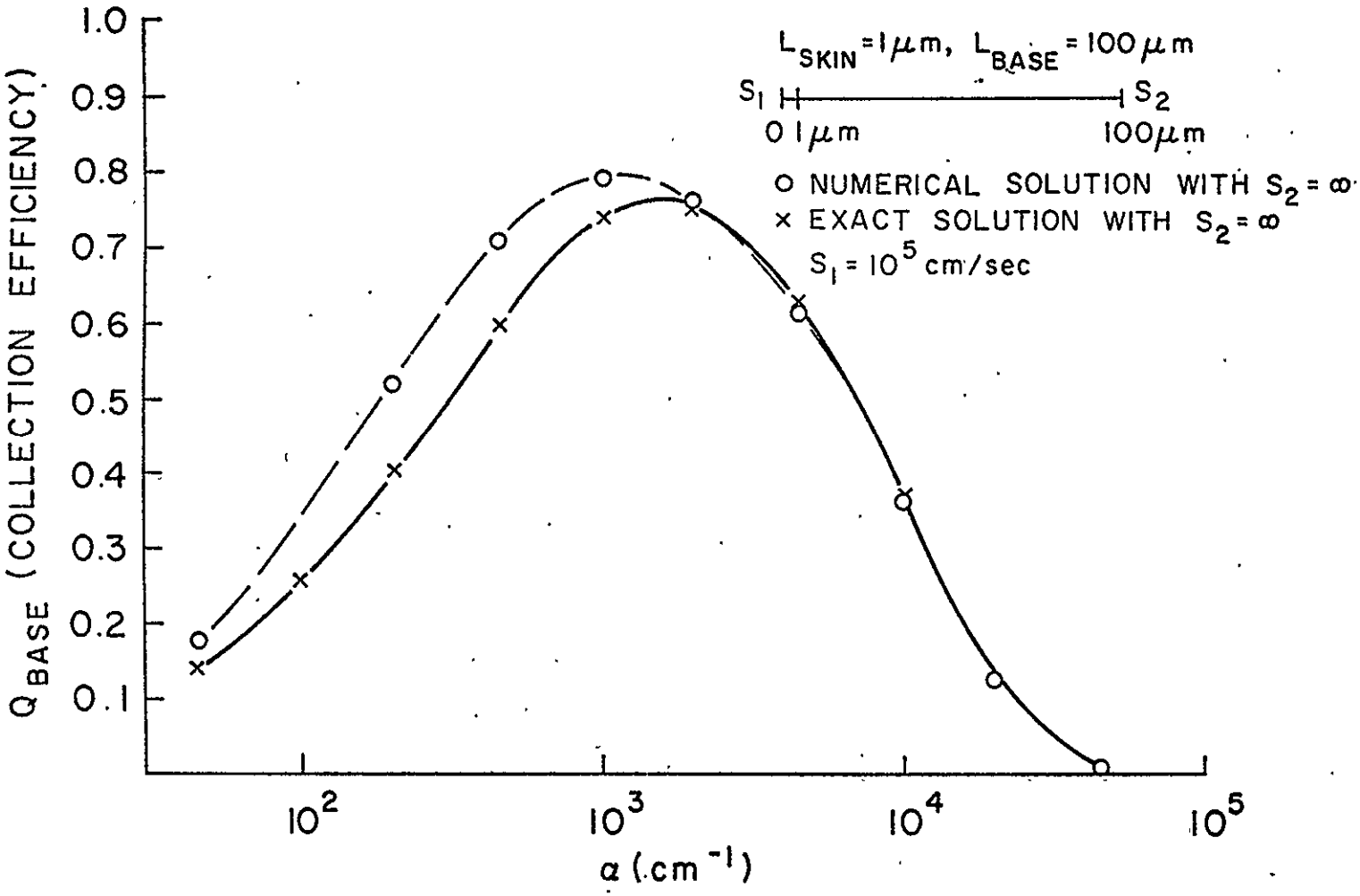

FIG.4 BASE COLLECTION EFFICIENCY AS OBTAINED FROM A NUMERICAL AND THE EXACT SOLUTIONS OF A ONE DIMENSIONAL CELL.

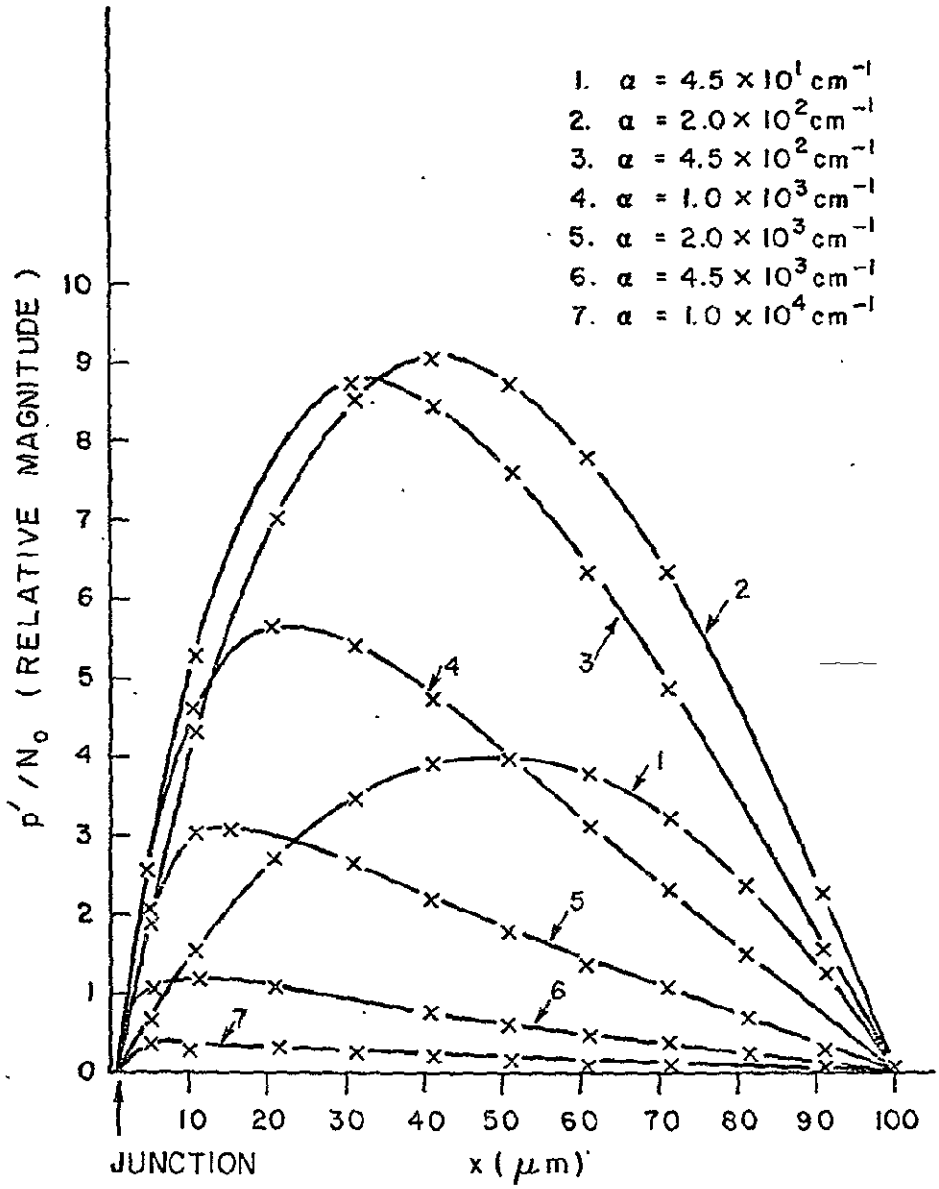

FIG.5 EXCESS MINORITY CHARGE CARRIER DISTRIBUTION IN THE BASE REGION PER UNIT VOLUME PER INCIDENT PHOTON OF THE ONE DIMENSIONAL CELL AS SPECIFIED IN FIG. 4

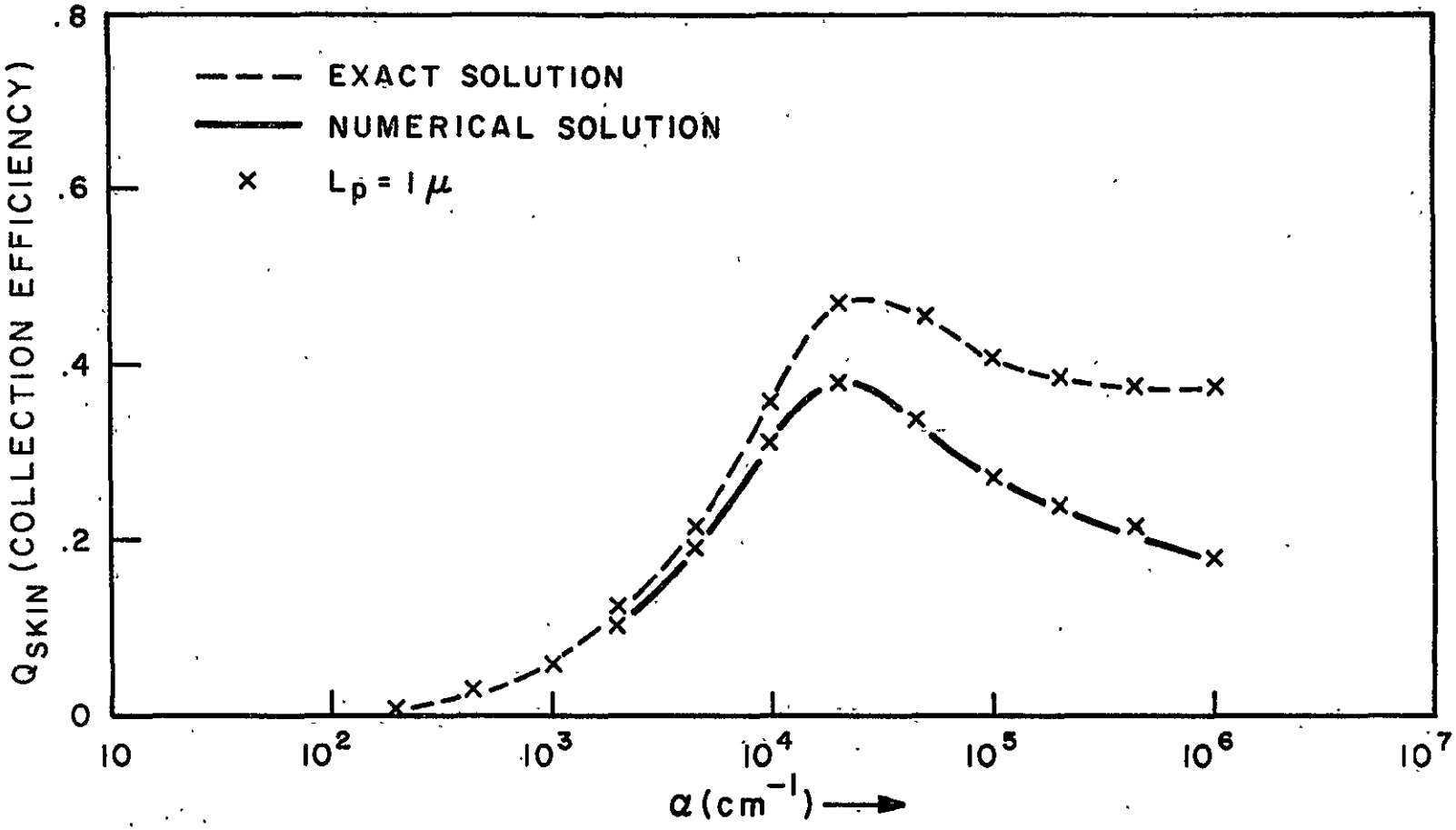

FIG. 6 SKIN COLLECTION EFFICIENCY AS OBTAINED FROM A NUMERICAL AND THE EXACT SOLUTIONS OF A ONE DIMENSIONAL CELL AS SPECIFIED IN FIG. 4.

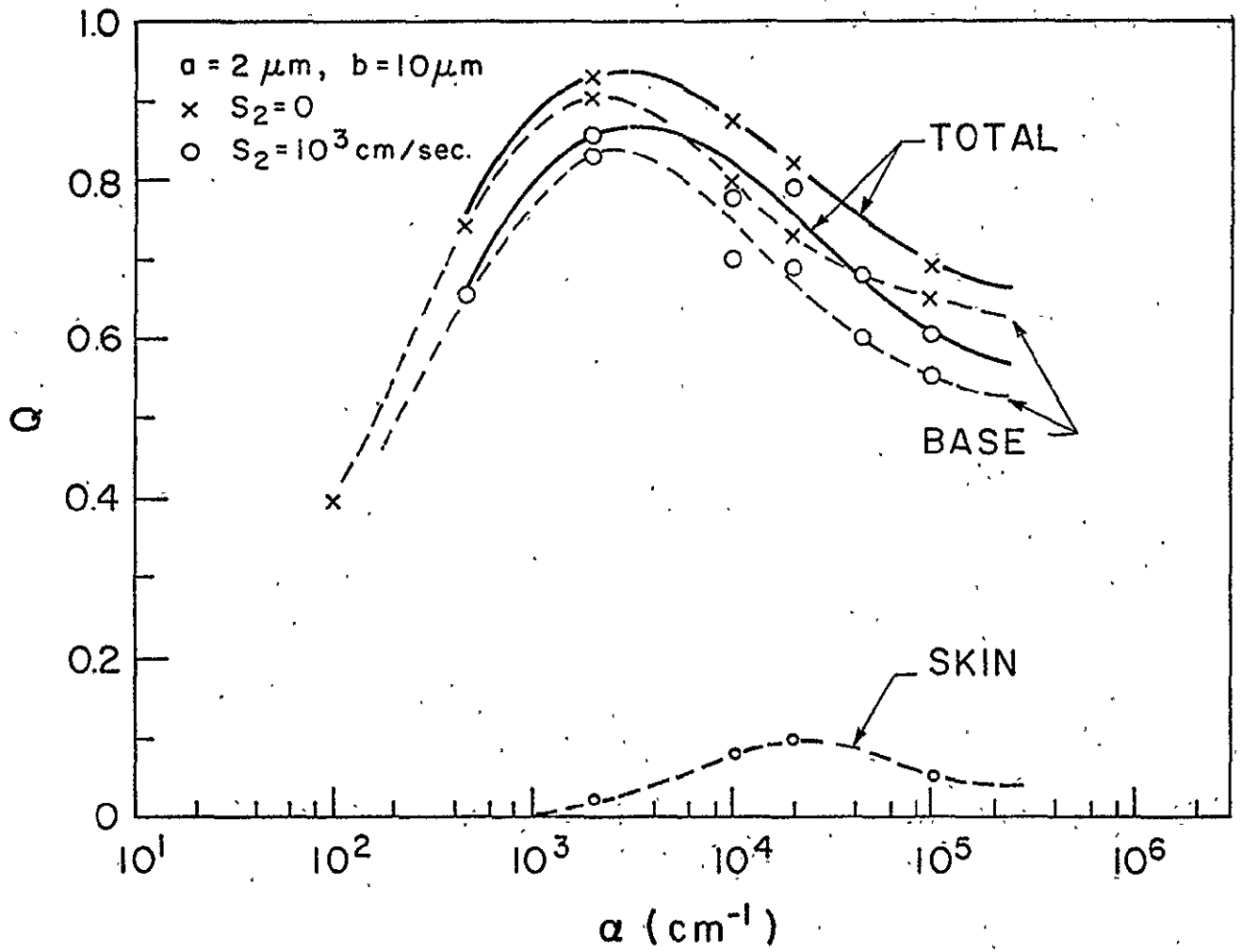

FIG. 7 CALCULATED COLLECTION EFFICIENCY OF A GRATING CELL WITH TWO DIFFERENT SURFACE RECOMBINATION VELOCITIES OF THE BASE MATERIAL.

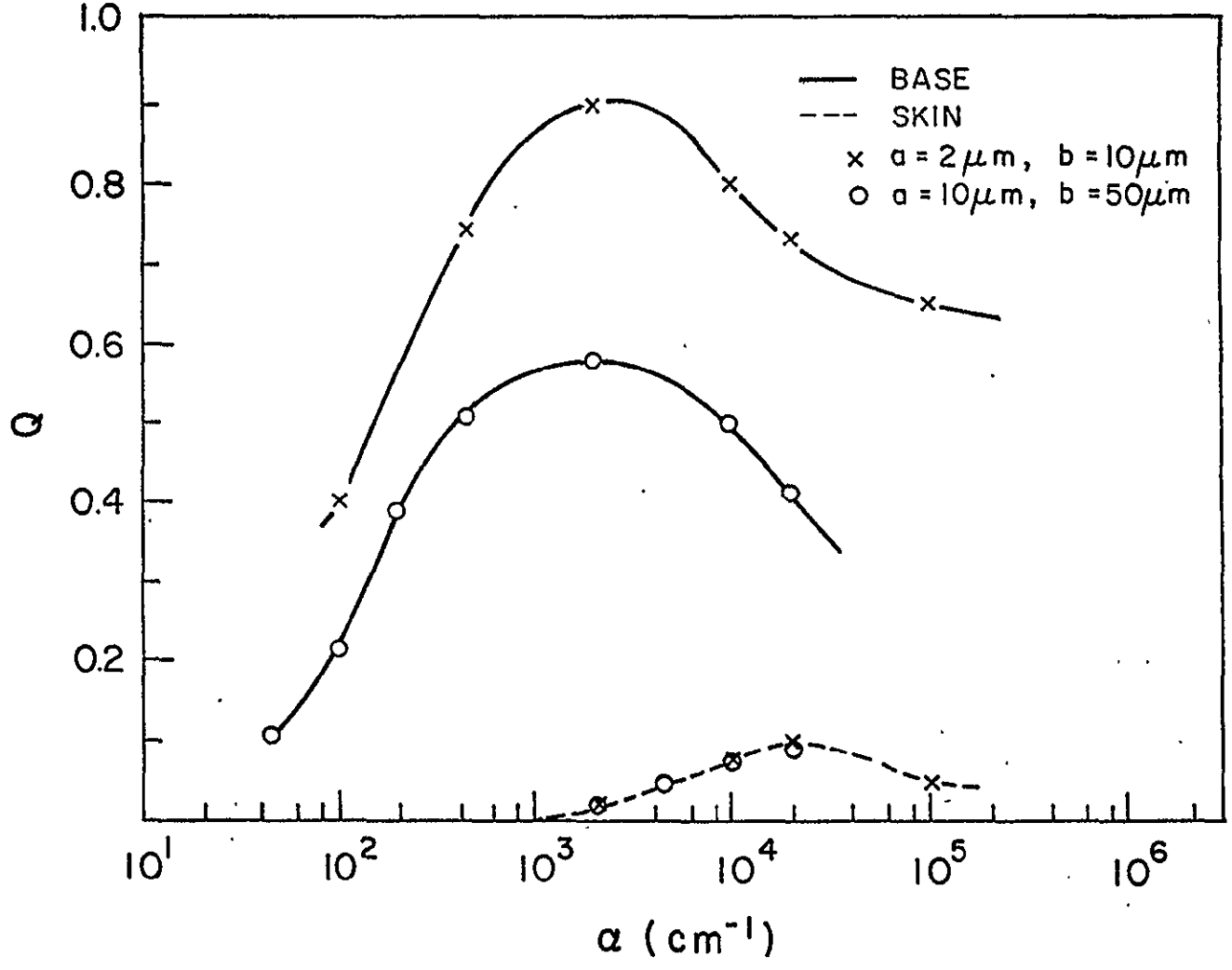

FIG.8 CALCULATED COLLECTION EFFICIENCY FOR GRATING CELLS WITH FIXED b/a=5 AND a=2μm, 10μm RESPECTIVELY.

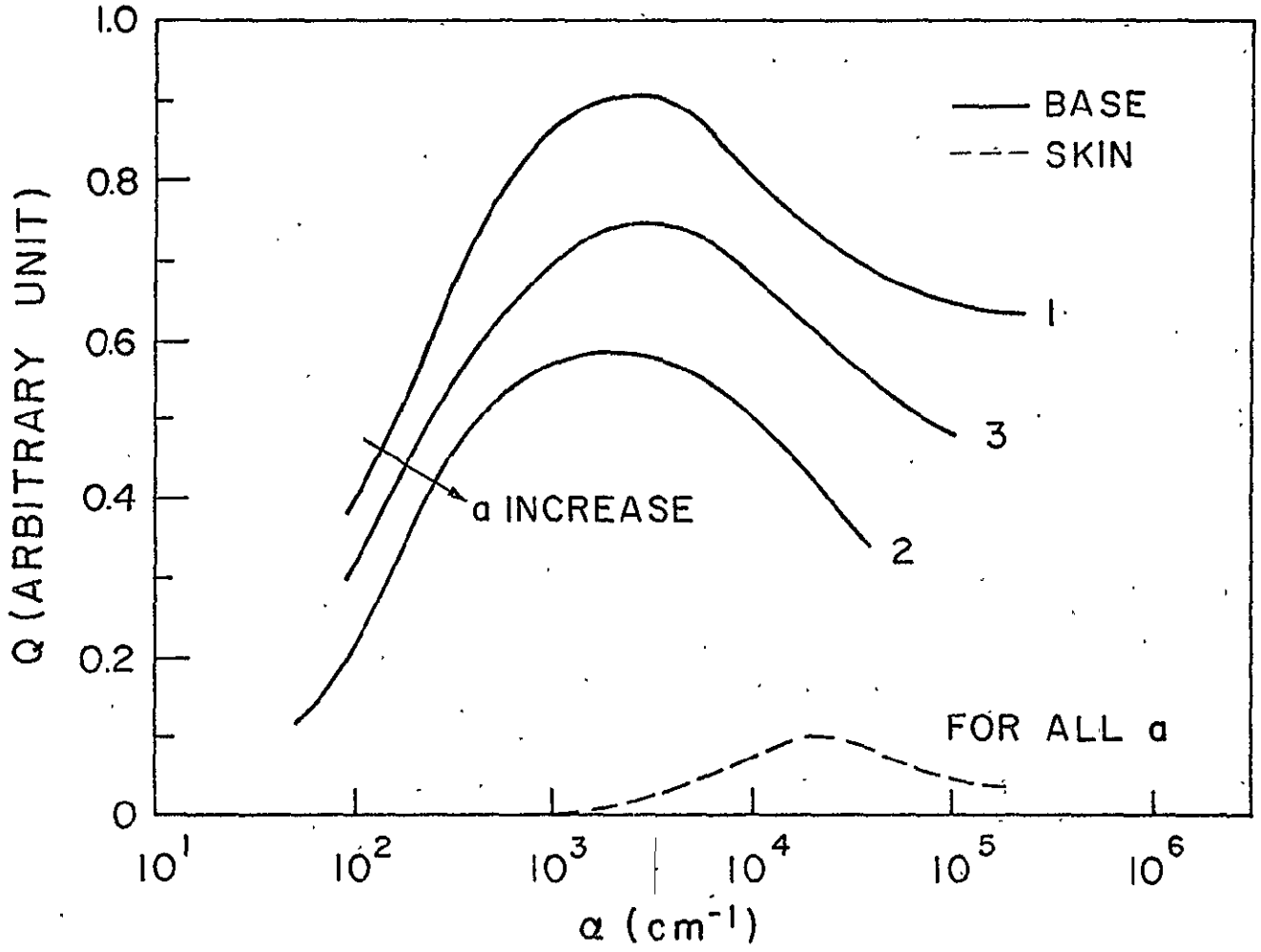

FIG. 9 A QUALITATIVE DESCRIPTION OF THE COLLECTION EFFICIENCY FOR GRATING CELLS WITH A FIXED VALUE OF b/a AND DIFFERENT VALUES OF a

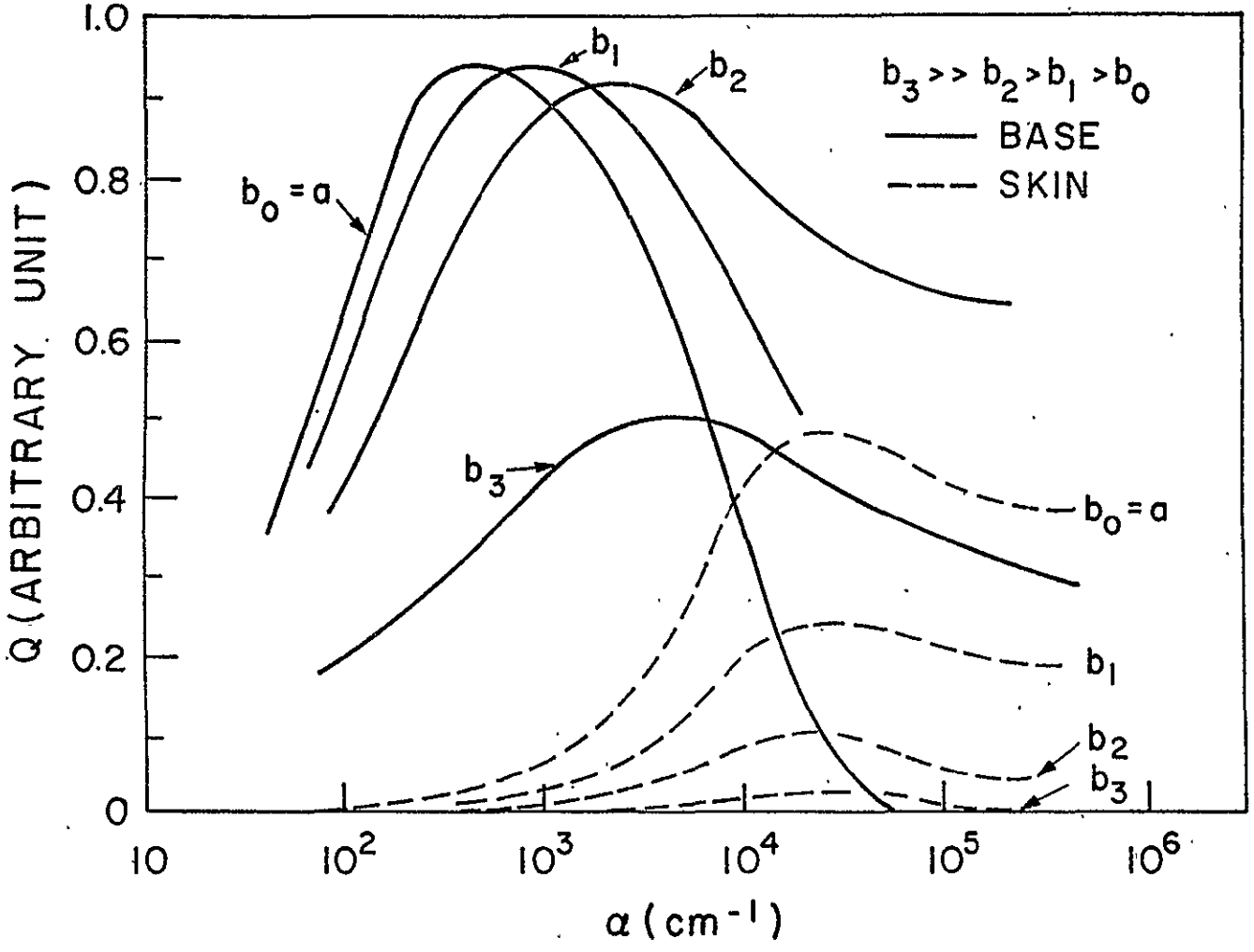

FIG. 10 A QUALITATIVE DESCRIPTION OF THE COLLECTION EFFICIENCY FOR GRATING CELLS WITH A FIXED VALUE OF a AND DIFFERENT VALUES OF b.

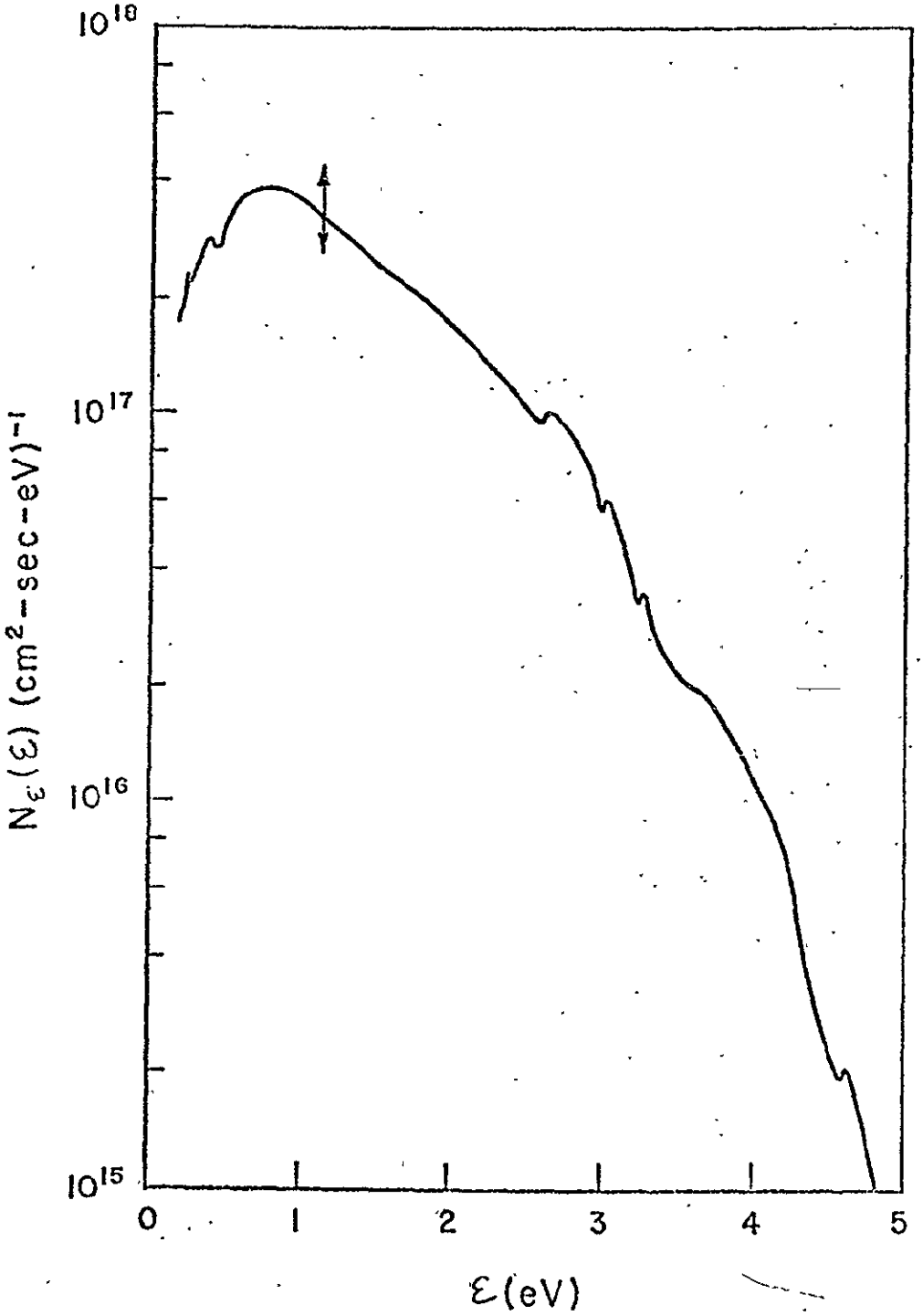

FIG.11 NUMBER OF PHOTONS AVAILABLE OUTSIDE THE EARTH'S ATMOSPHERE AS A FUNCTION OF PHOTON ENERGY.

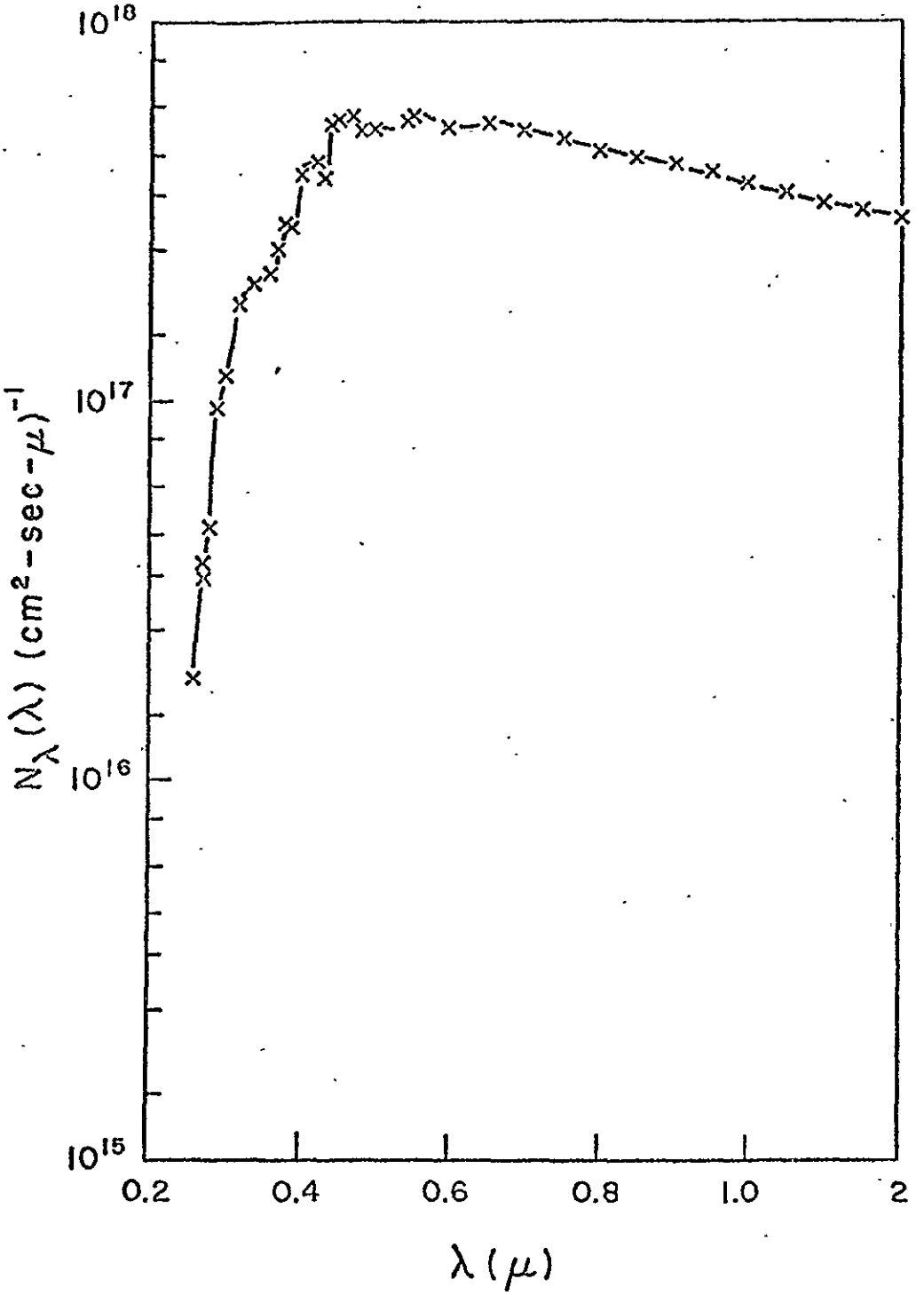

FIG. 12 NUMBER OF PHOTONS AVAILABLE OUTSIDE THE EARTH'S ATMOSPHERE AS A FUNCTION OF PHOTON WAVE-LENGTH.

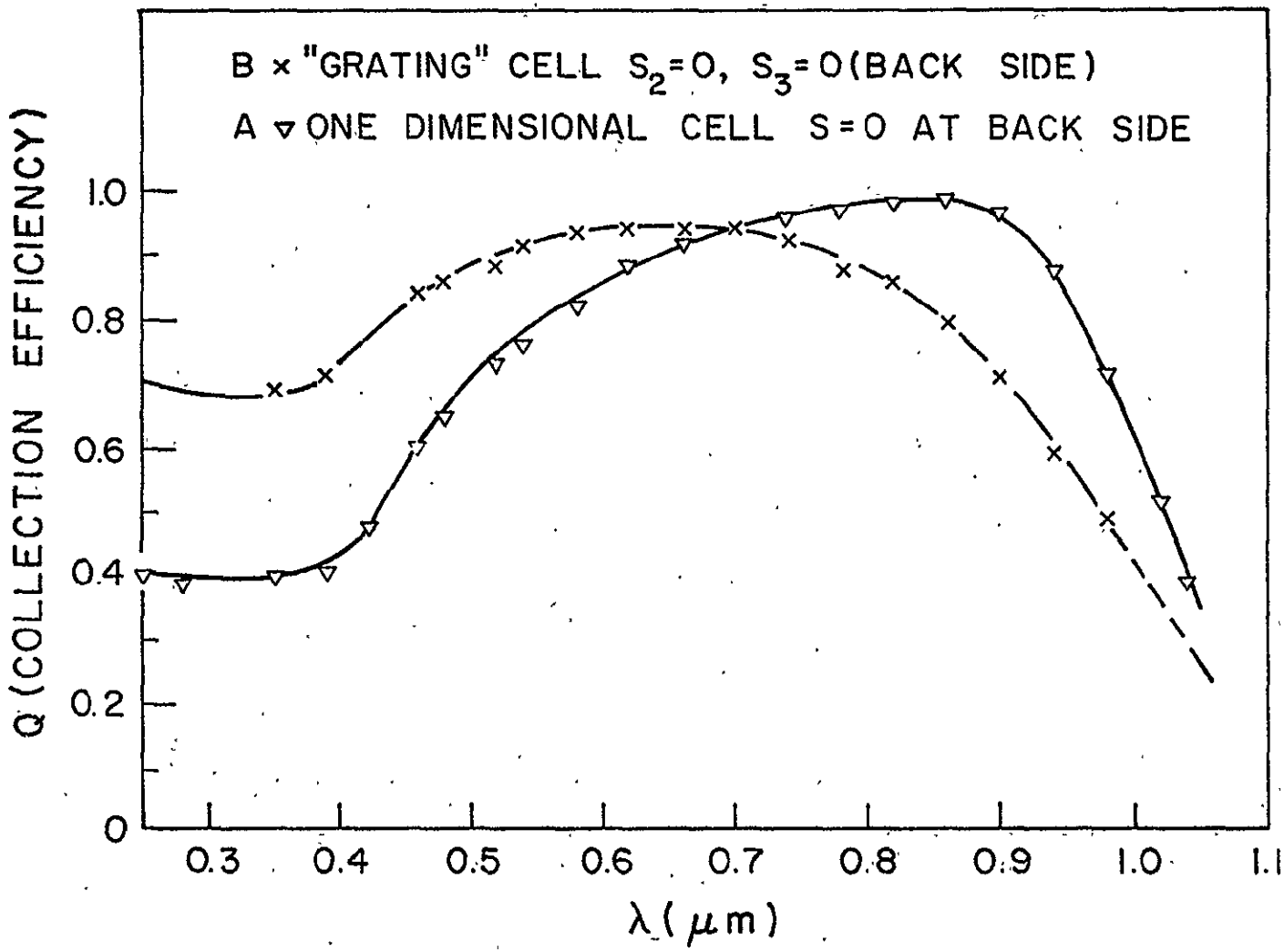

FIG. 13 COLLECTION EFFICIENCY OF GRATING CELL AND A CORRESPONDING CONVENTIONAL CELL AS A FUNCTION OF PHOTON WAVELENGTH

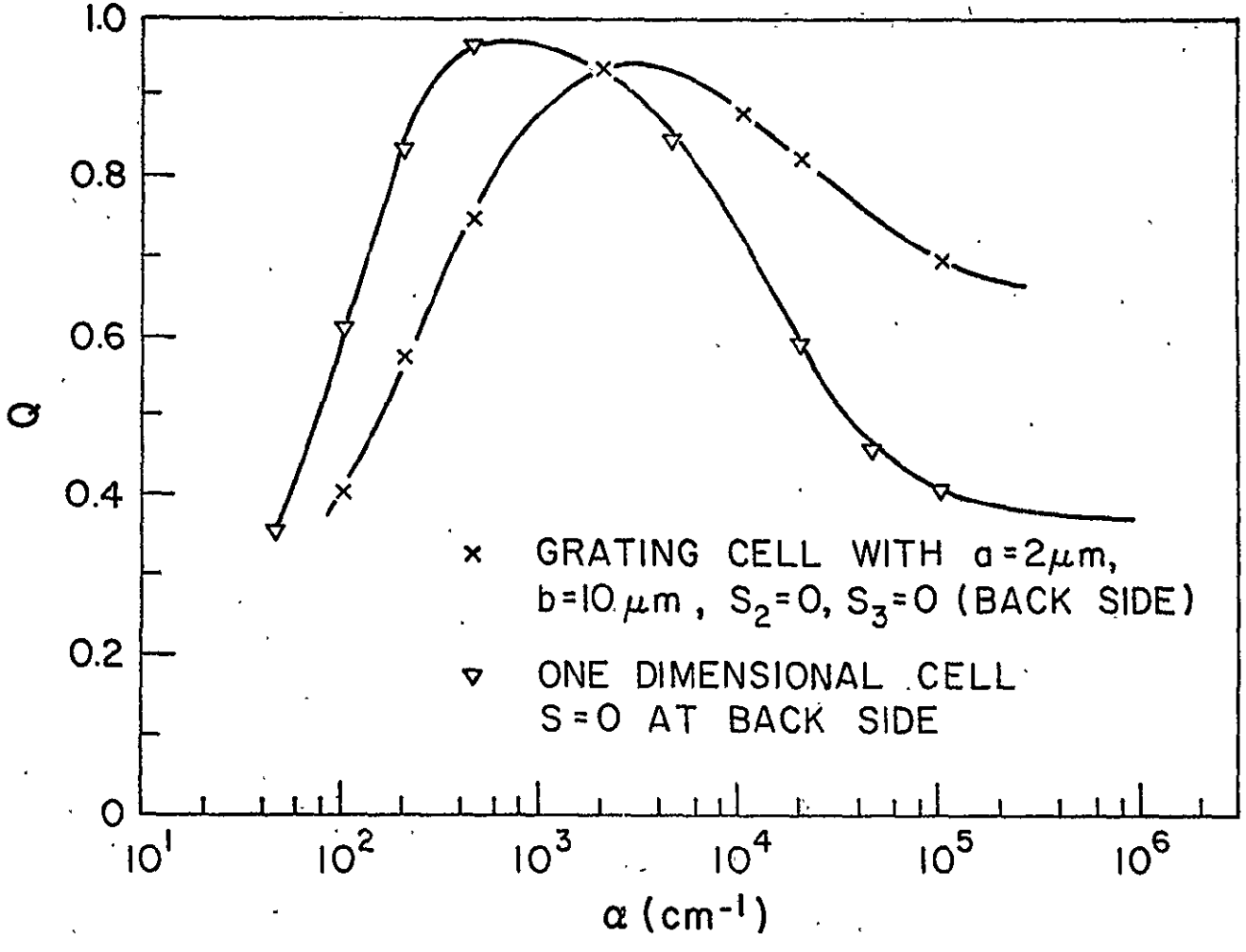

FIG.14 COLLECTION EFFICIENCY OF A GRATING CELL AND A CORRESPONDING CONVENTIONAL CELL AS A FUNCTION OF THE OPTICAL ABSORPTION CONSTANT

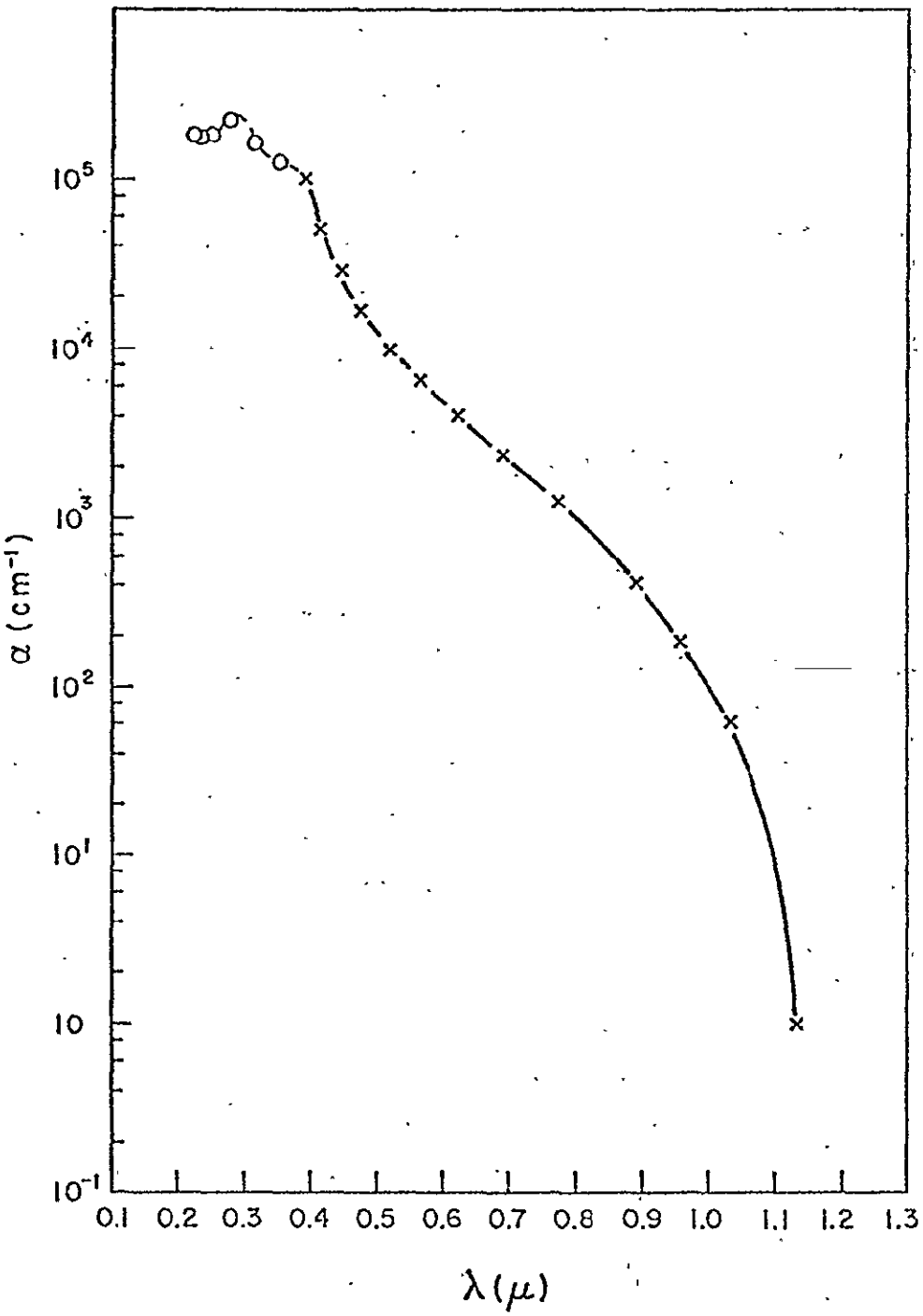

FIG. 15 ABSORPTION SPECTRA OF SINGLE CRYSTAL SILICON AT 300°K.

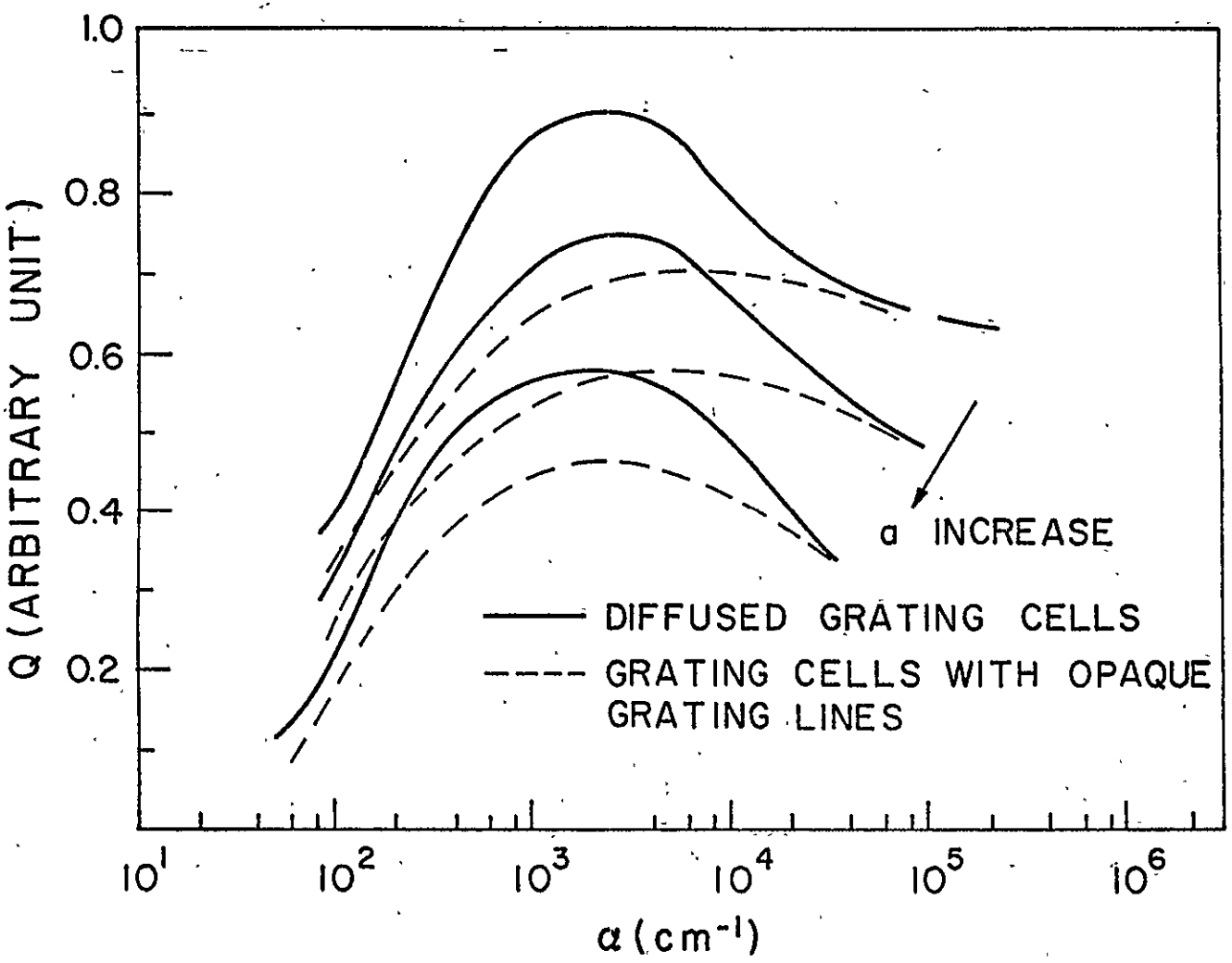

FIG. 16 A QUALITATIVE DESCRIPTION OF THE BASE COLLECTION EFFICIENCY OF GRATING CELLS WITH OPAQUE GRATING LINES. b/a = CONSTANT.

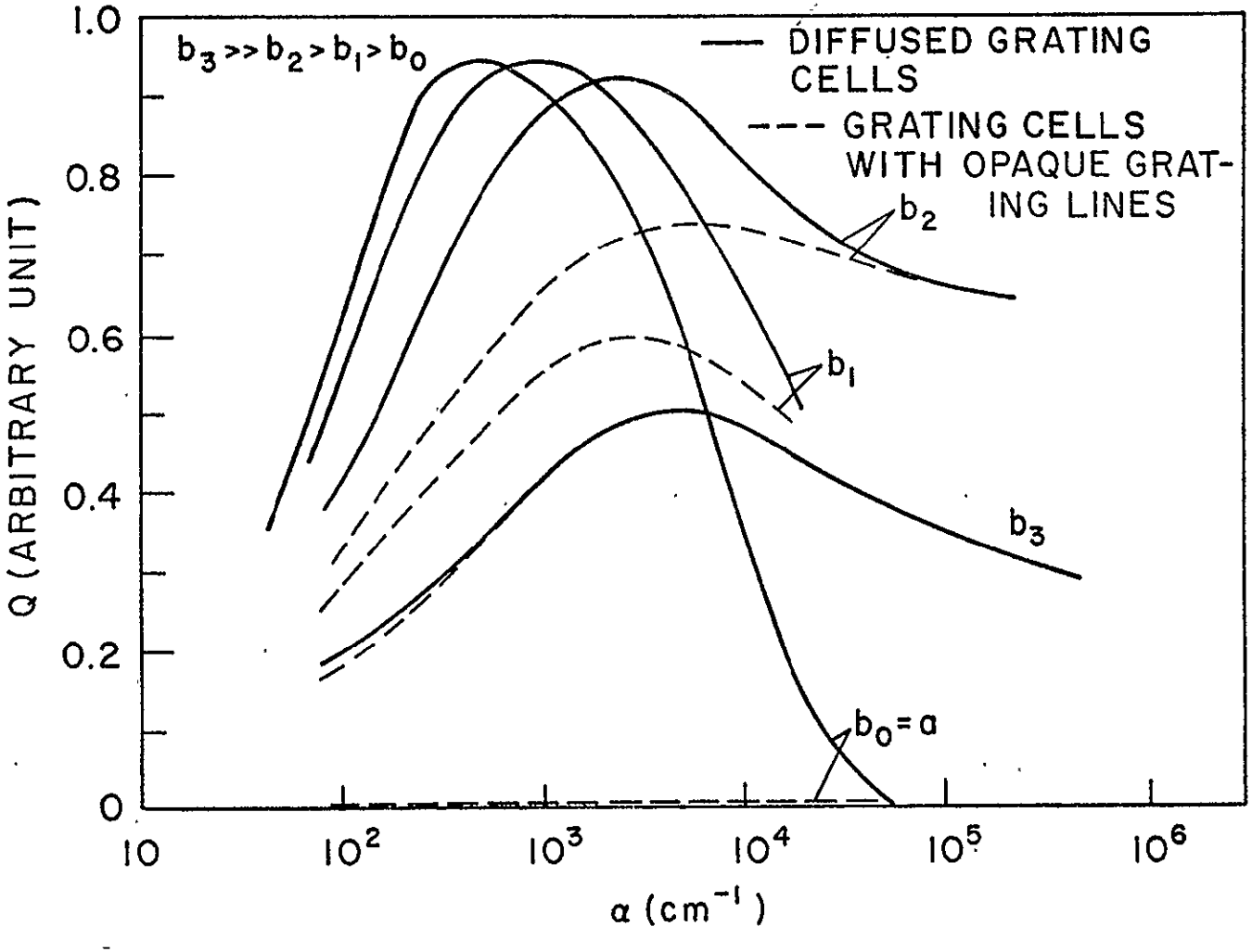

FIG. 17 A QUALITATIVE DESCRIPTION OF THE BASE COLLECTION EFFICIENCY OF GRATING CELLS WITH OPAQUE GRATING LINES. a = CONSTANT.

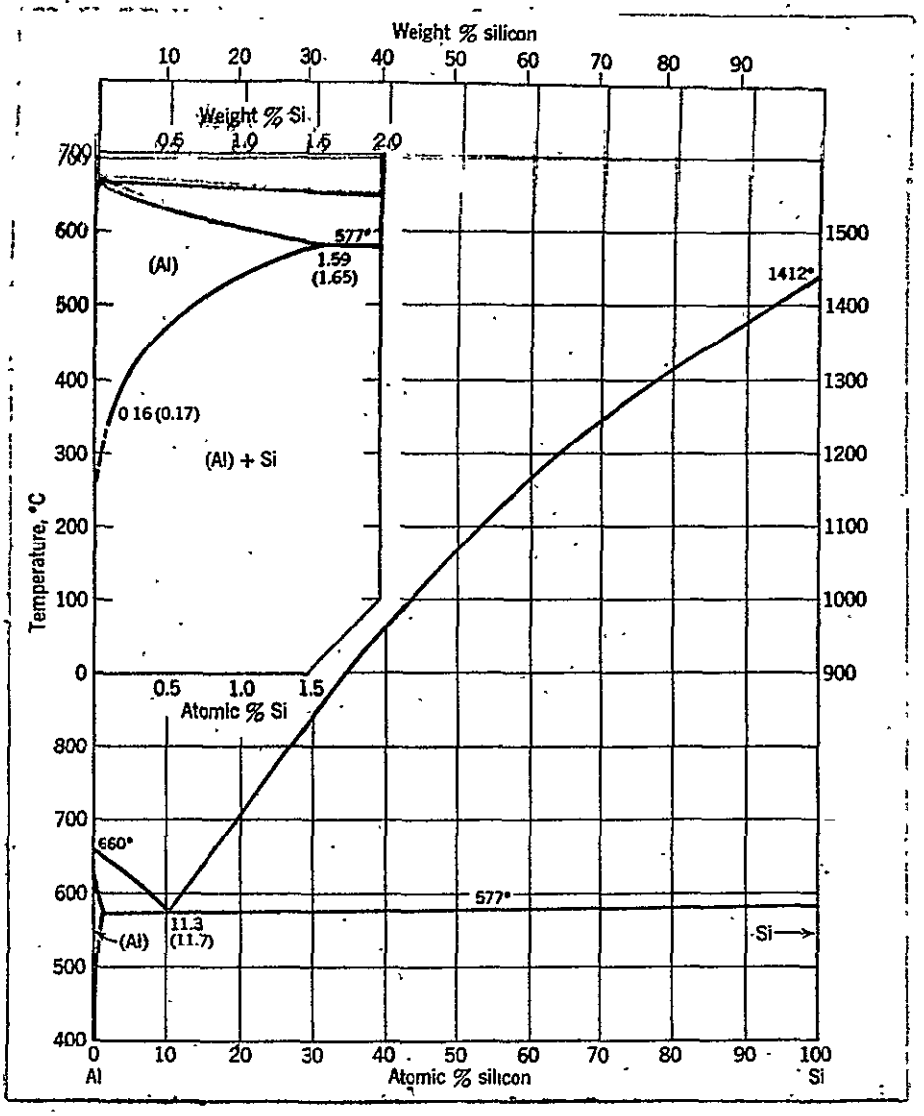

FIG. 18 THE ALUMINUM - SILICON SYSTEM (FROM M. HANSEN, AND A. ANDERKO, CONSTITUTION OF BINARY ALLOYS, McGRAW - HILL, NEW YORK, 1958.)

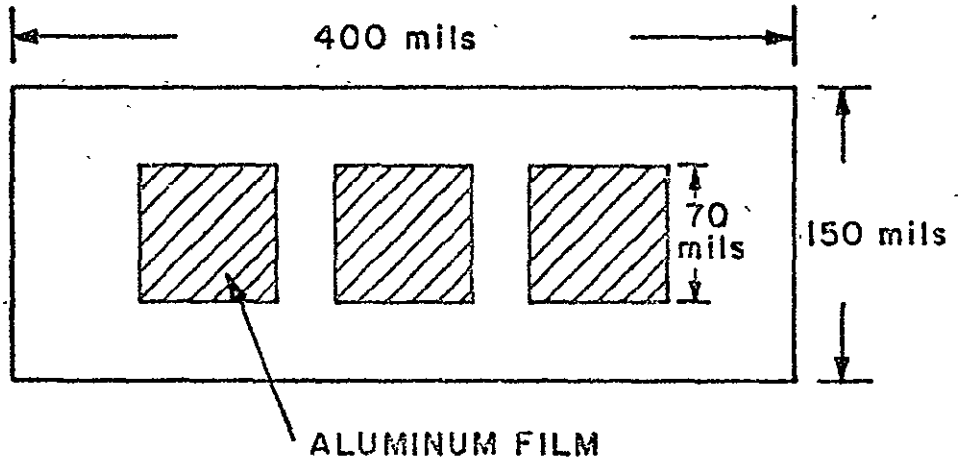

FIG. 19 TEST SAMPLE CONFIGURATION.

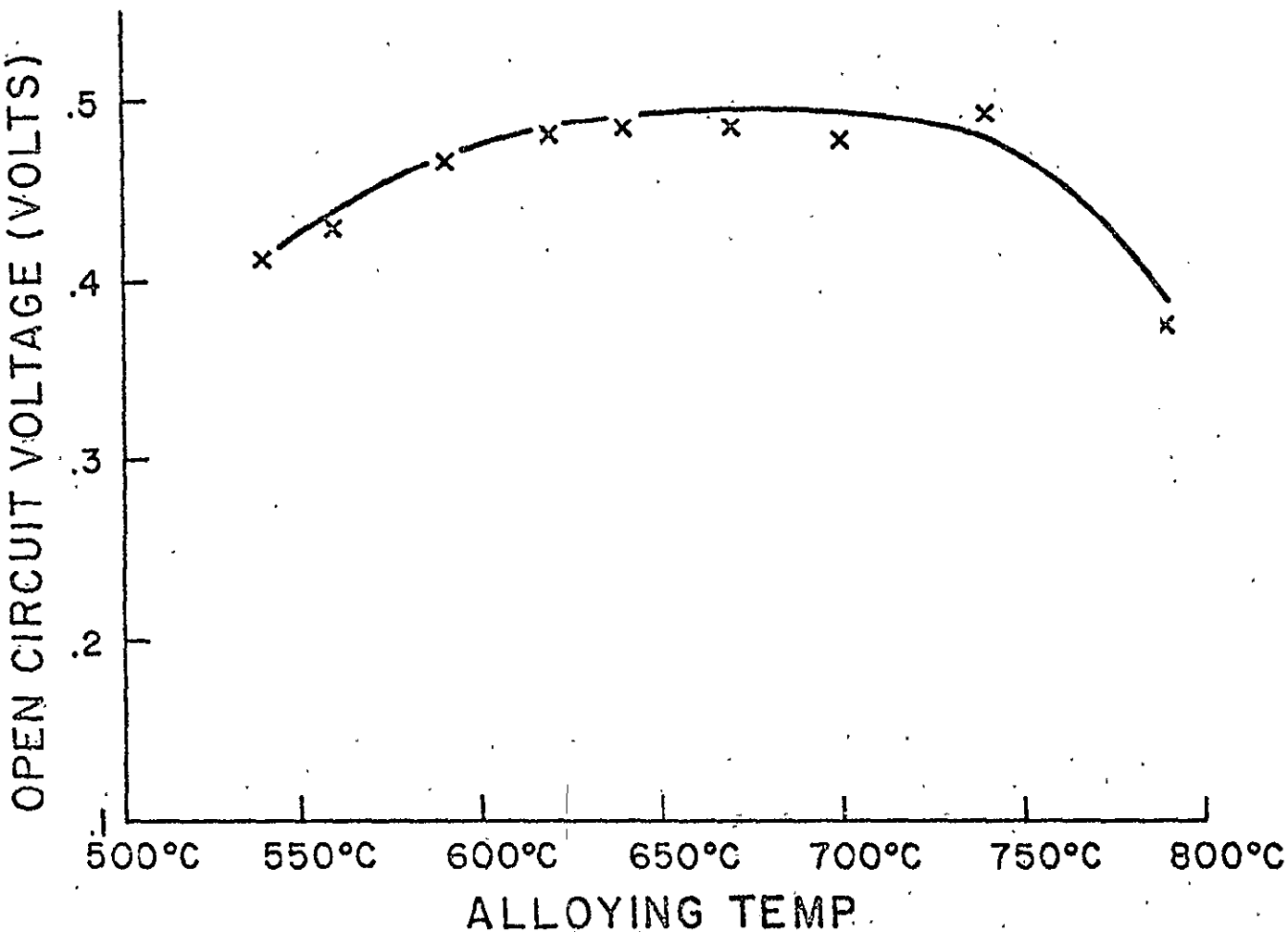

FIG. 20 OPEN CIRCUIT VOLTAGE VERSUS ALLOYING TEMPERATURE.

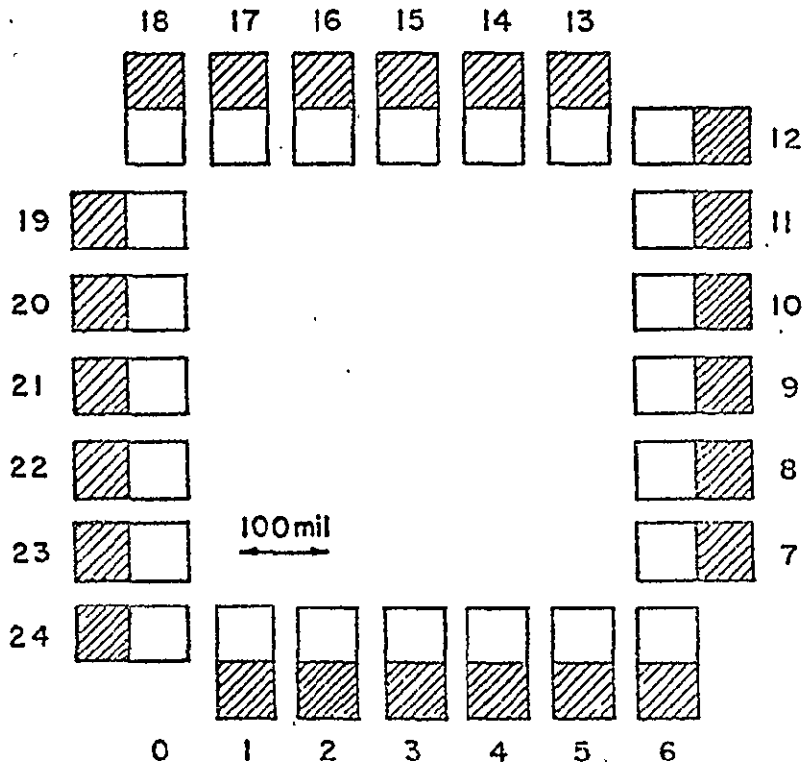

MAGNIFIED VIEW OF A SINGLE CELL.

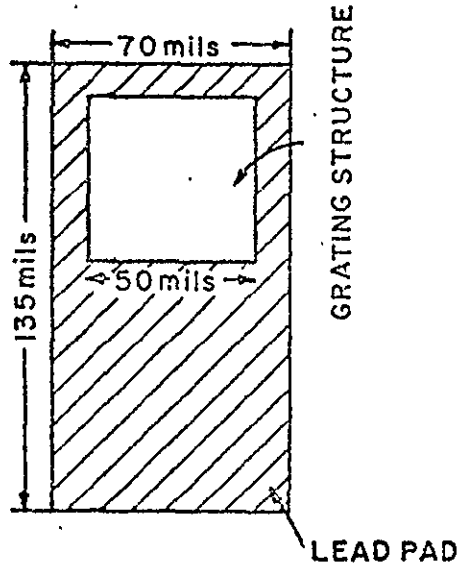

FIG. 21 CONFIGURATION OF CELLS PRODUCED ON A SINGLE WAFER.

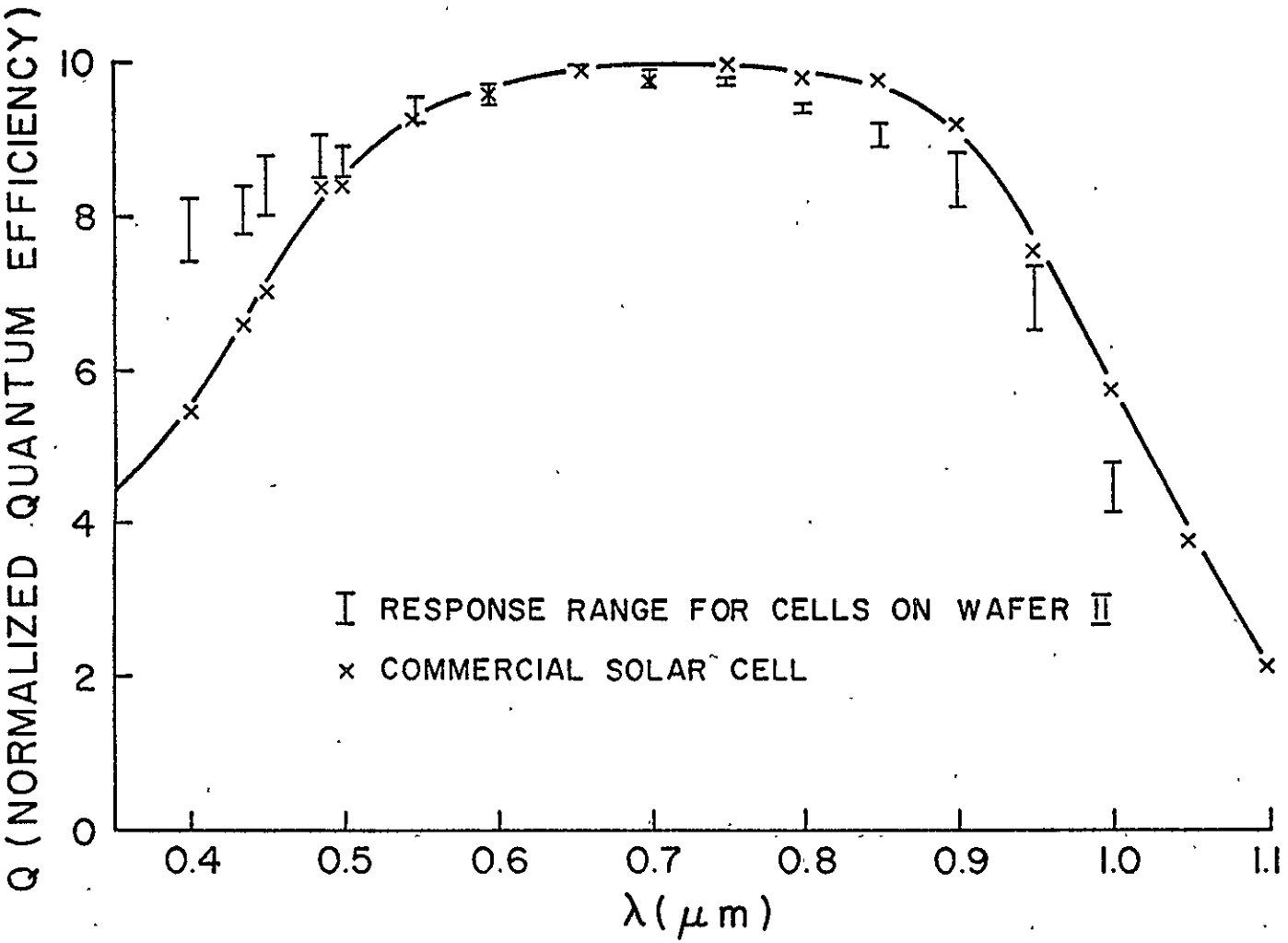

FIG. 22 NORMALIZED SPECTRAL RESPONSES FOR CELLS ON WAFER II AND A COMMERCIAL SOLAR CELL WITH AR COATING REMOVED

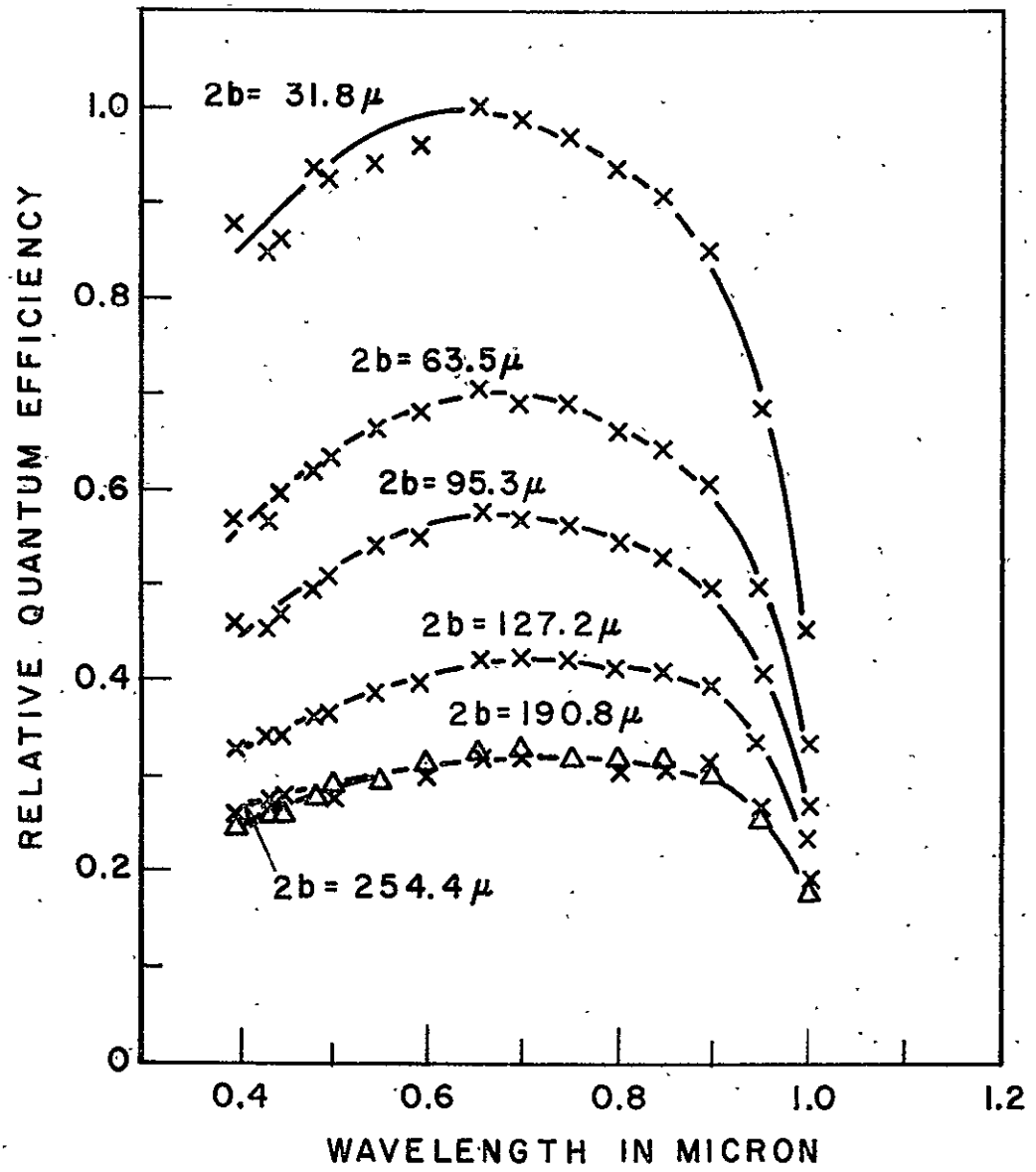

FIG.23 RELATIVE SPECTRAL RESPONSES FOR CELLS ON WAFER I. $2a = 5.1\mu m$, I_{sc} (max) = 9.46 mA/cm^2.

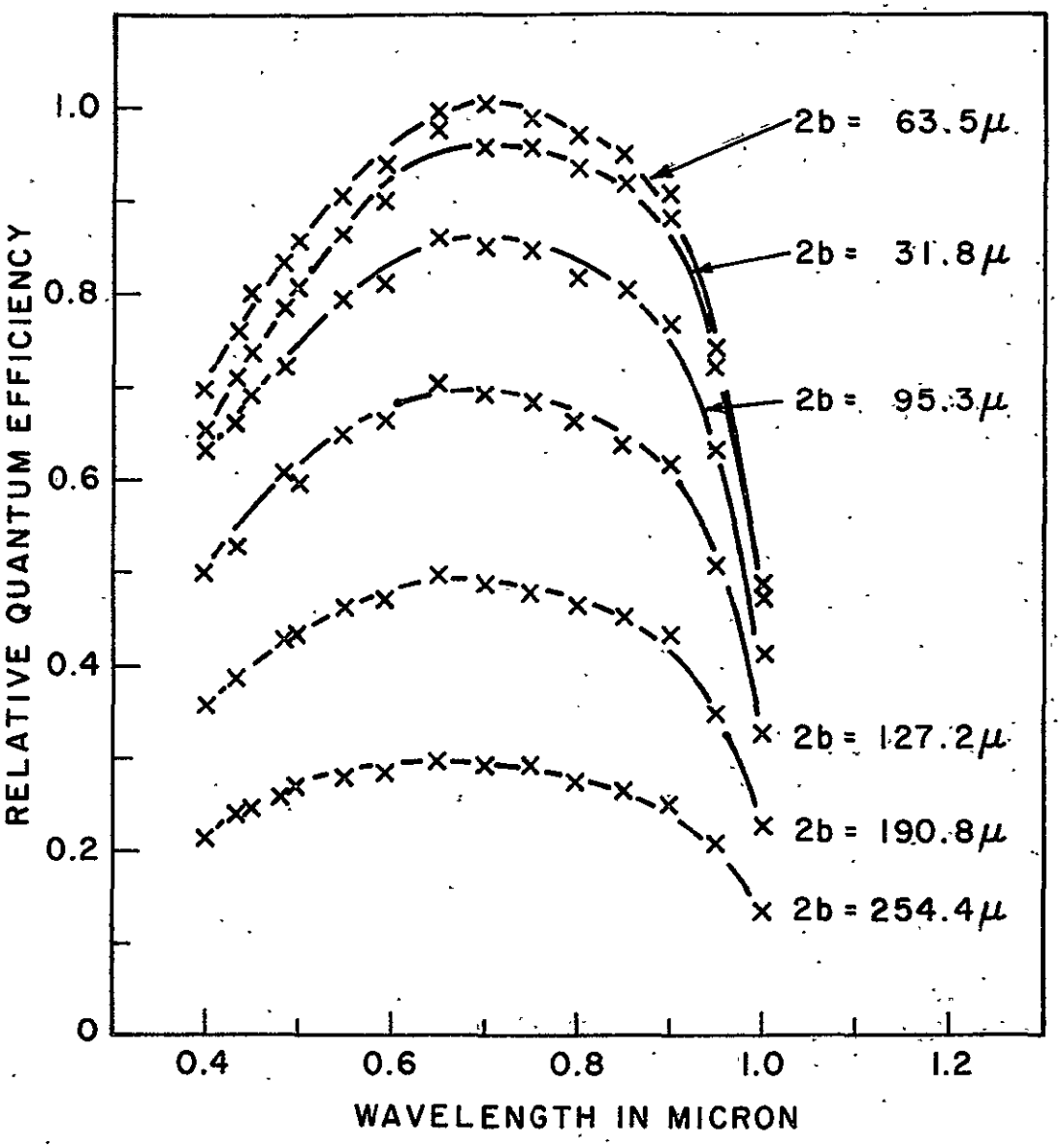

FIG.24 RELATIVE SPECTRAL RESPONSES FOR CELLS ON WAFER III. $2a = 5.1\mu m$, I_{sc} (max) = 23.9 mA/cm^2.

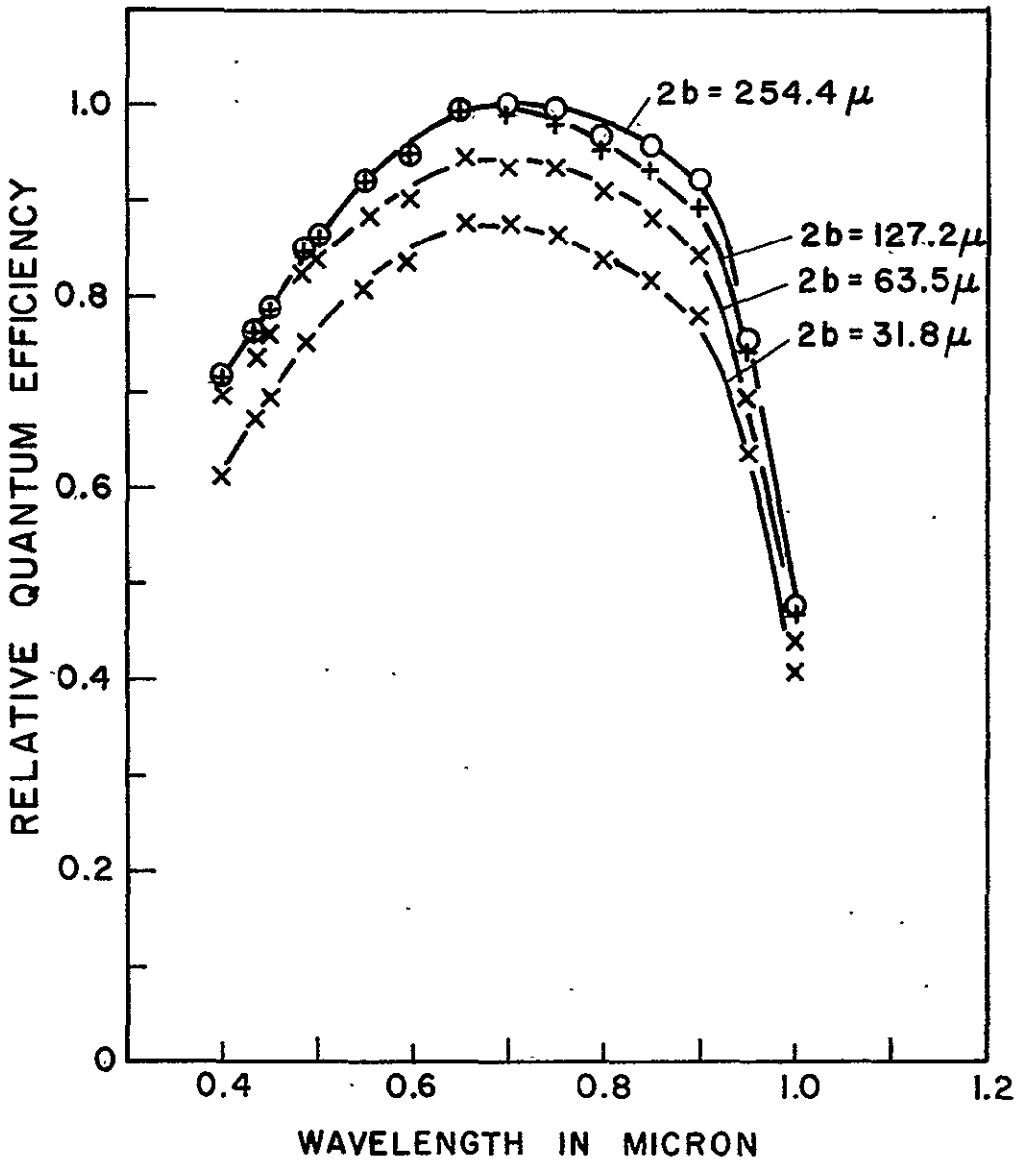

FIG. 25 RELATIVE SPECTRAL RESPONSES FOR CELLS ON WAFER V. $2a = 5.1\mu m$, $I_{sc}(max) = 28.8\ mA/cm^2$.

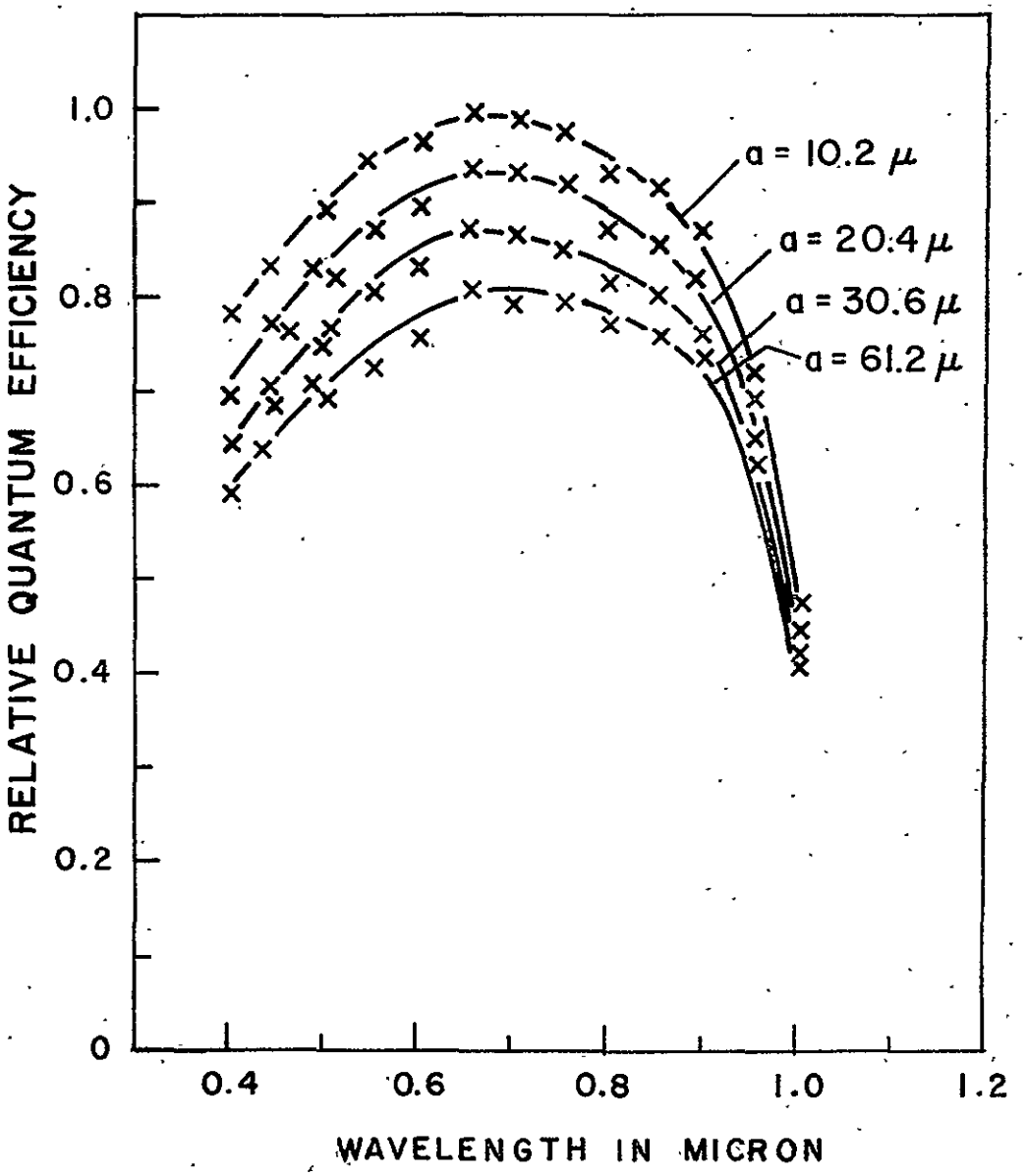

FIG. 26 RELATIVE SPECTRAL RESPONSES FOR CELLS ON WAFER VI. a : b = 8 : 25

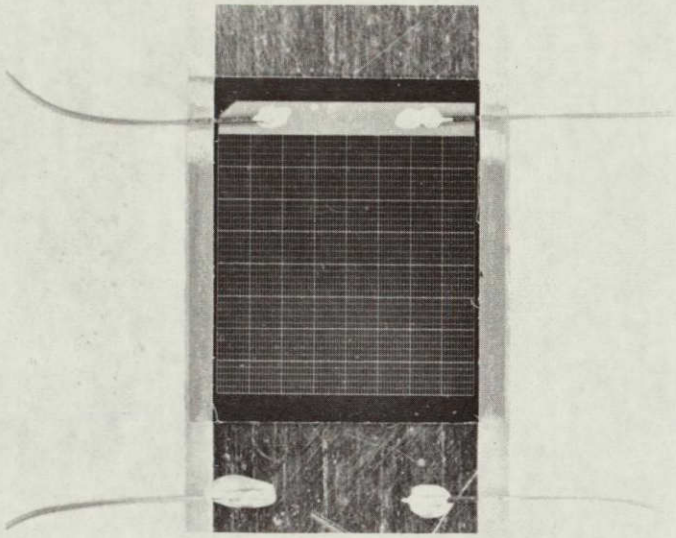

FIG. 27 A 1-cm^2 GRATING STRUCTURE CELL, $2a = 7.5\,\mu m$, $2b = 127.2\,\mu m$.

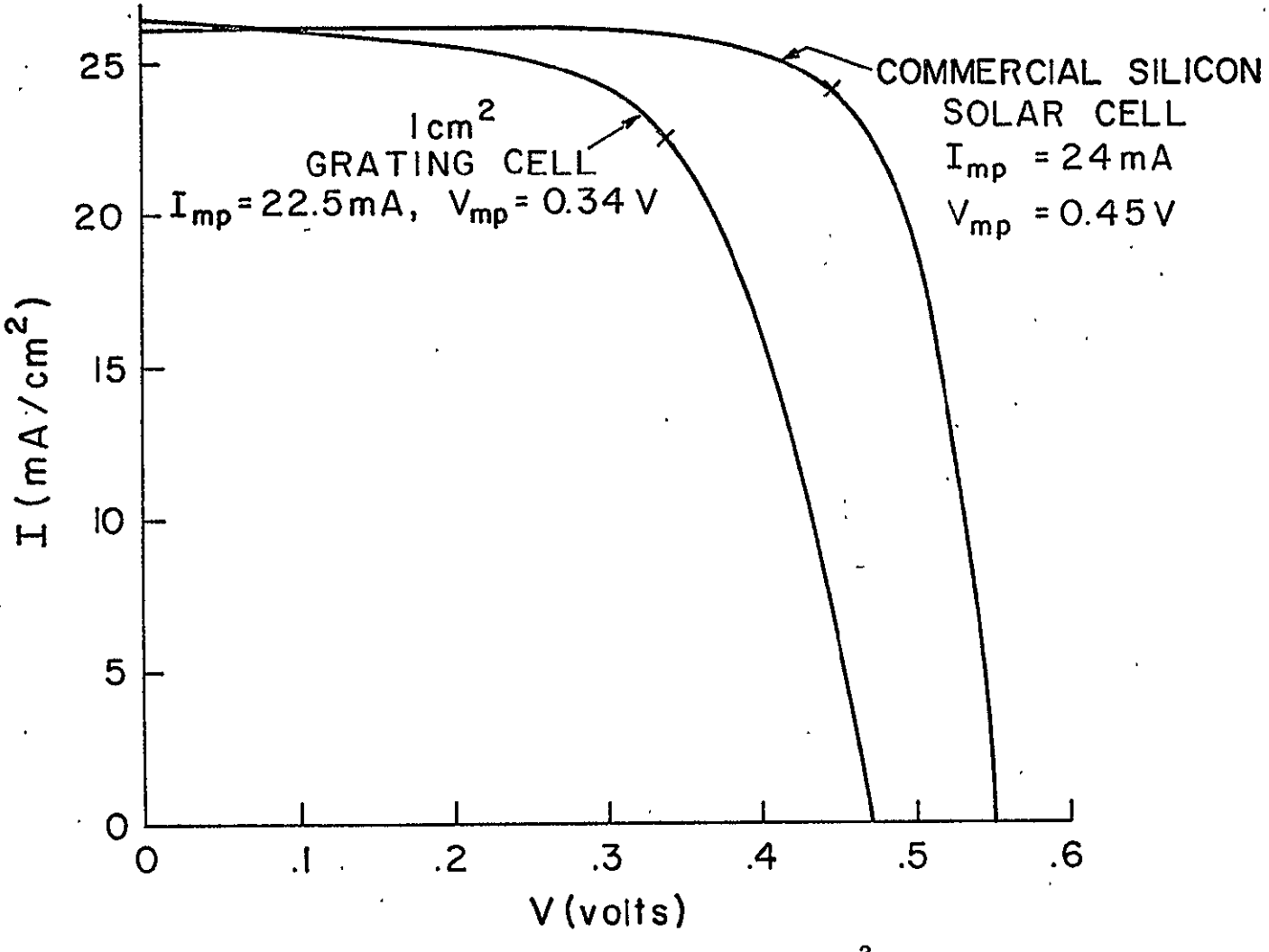

FIG. 28 I-V CHARACTERISTIC OF A 1-cm² GRATING CELL UNDER SIMULATED AMD ILLUMINATION

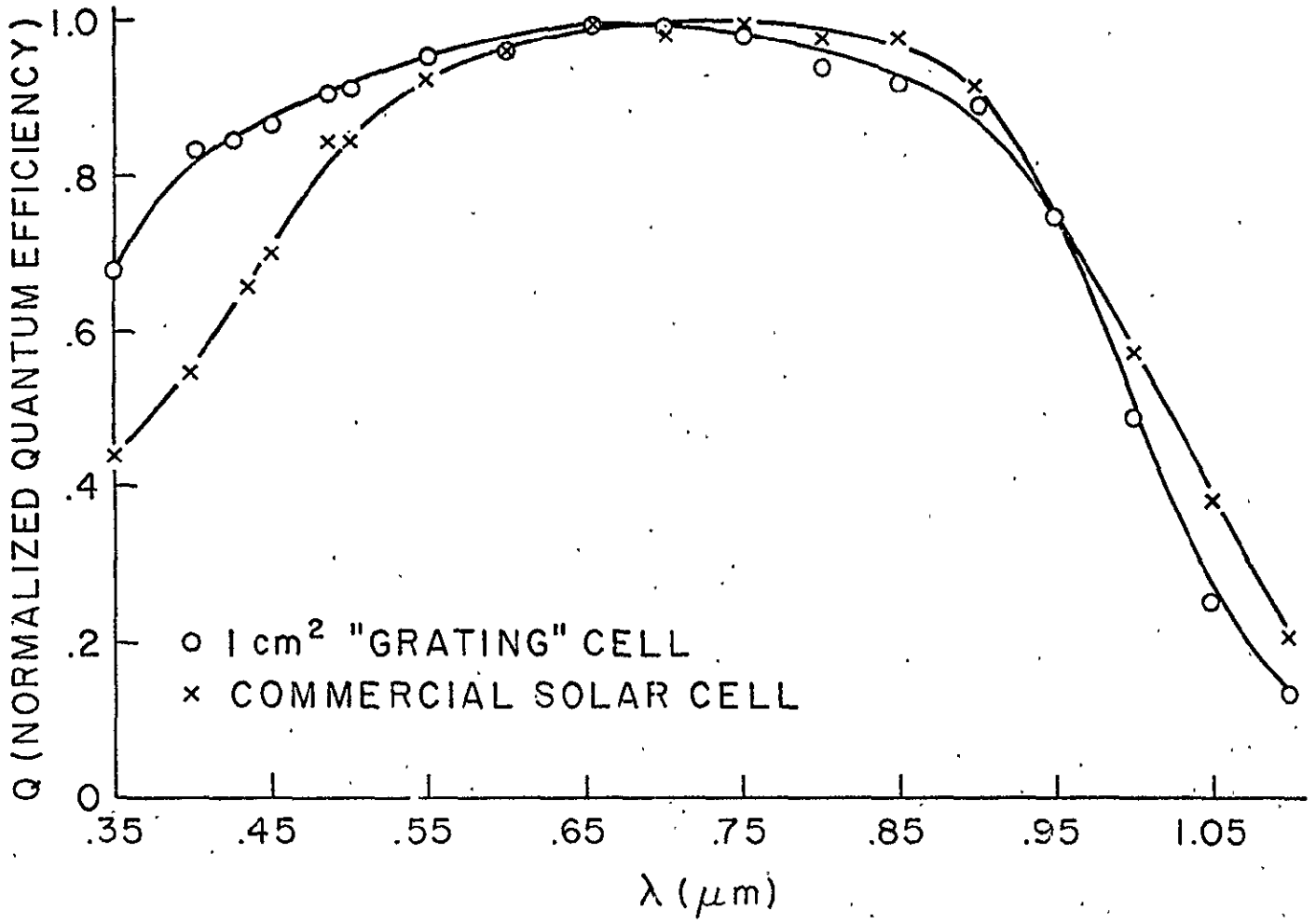

FIG. 29 NORMALIZED SPECTRAL RESPONSE OF A 1-cm² GRATING CELL.

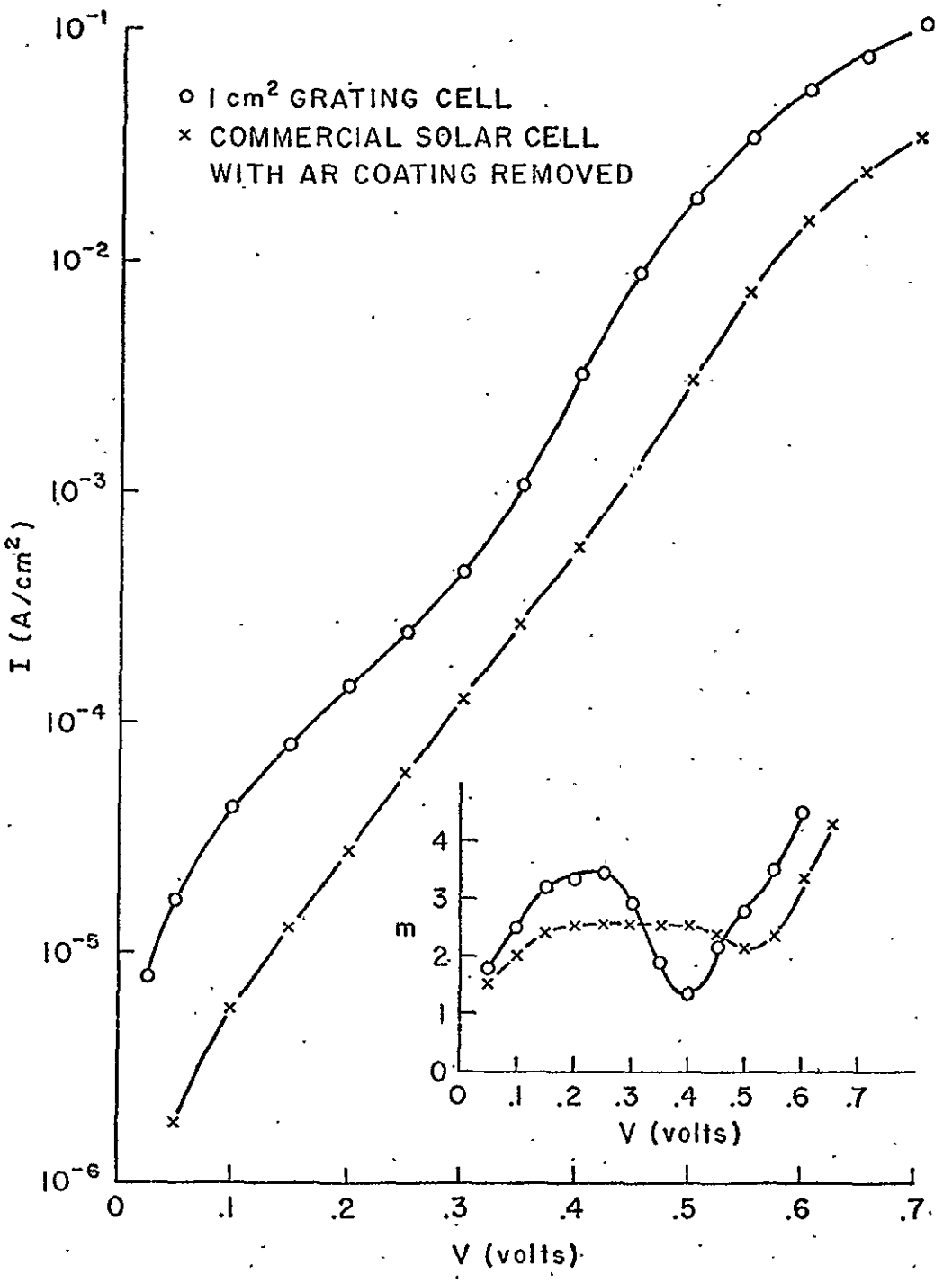

FIG. 30 DARK FORWARD I-V CHARACTERISTIC AND RECIPROCAL SLOPE m vs V CURVE OF A 1-cm² GRATING CELL.

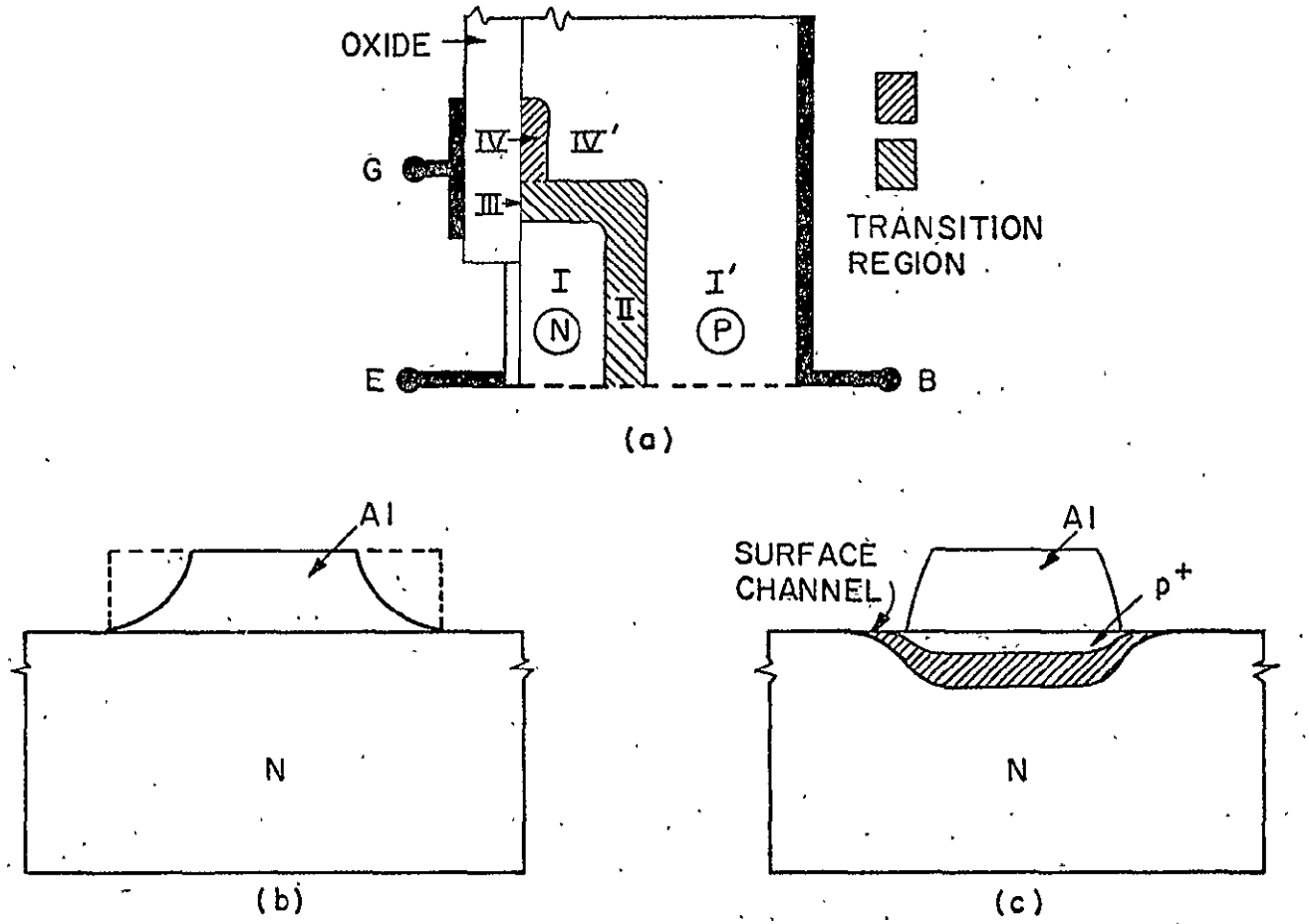

FIG. 31 DIAGRAMS USED TO ILLUSTRATE THE ORIGIN OF SURFACE CHANNEL NEAR A P-N JUNCTION.

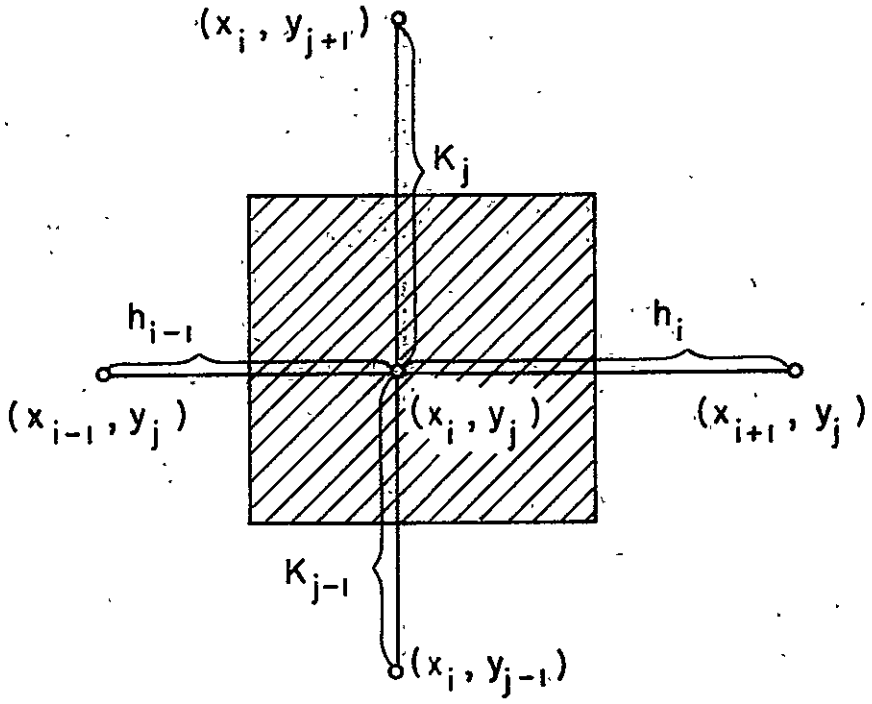

FIG. 32 FIVE POINT SCHEME OF THE FINITE DIFFERENCE METHOD

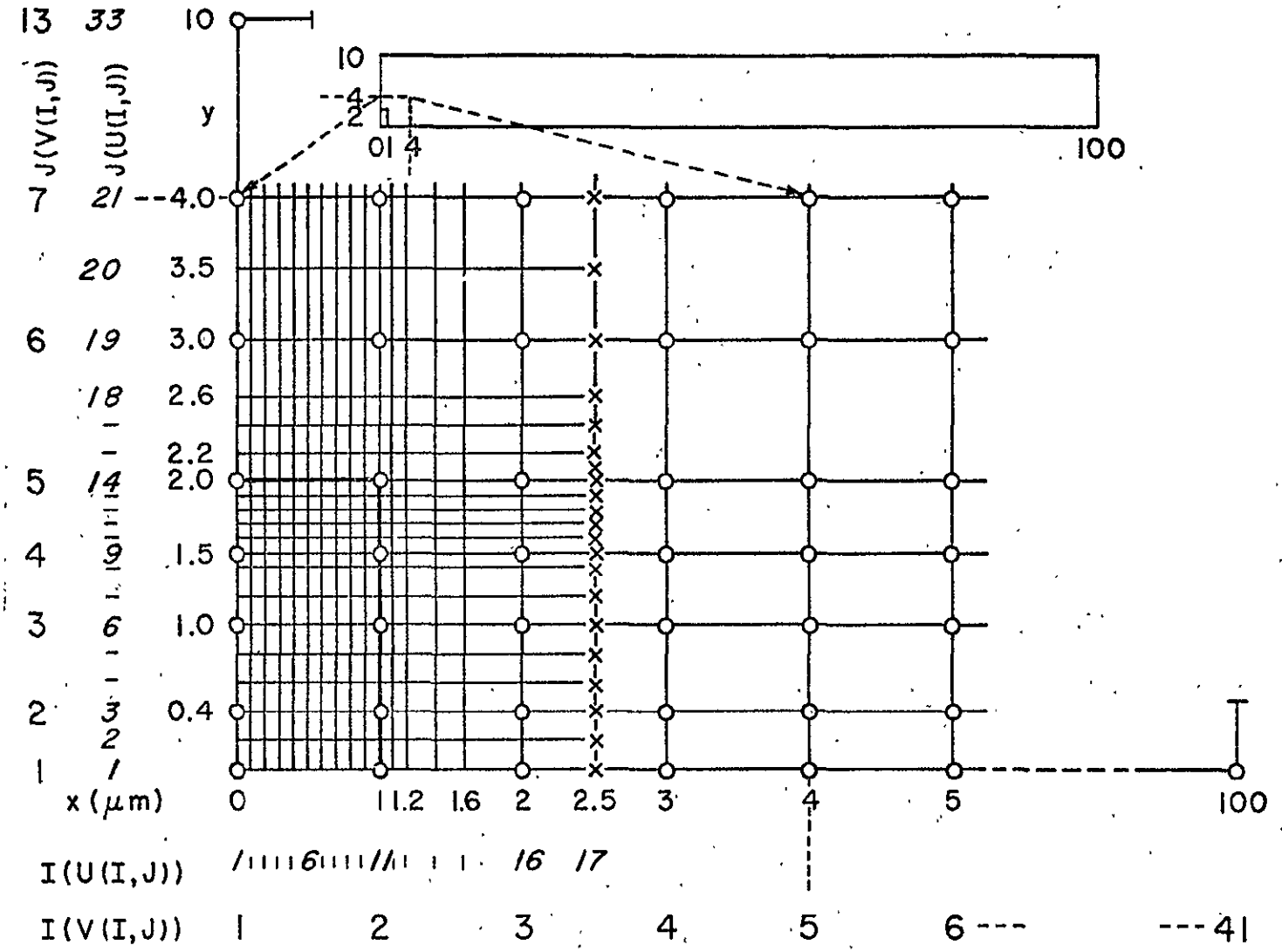

FIG. 33 DISCRETILIZATION OF THE UNIT CELL OF A GRATING CELL WITH $a = 2\,\mu m$, $b = 10\,\mu m$.